
Citation:

Stringer, CD and Carrivick, JL and Quincey, DJ and Nývlt, D and Comber, A (2025) Land cover change across the major proglacial regions of the sub-Antarctic islands, Antarctic Peninsula, and McMurdo Dry Valleys, during the 21st century. *Arctic, Antarctic, and Alpine Research*, 57 (1). pp. 1-25. ISSN 1523-0430 DOI: <https://doi.org/10.1080/15230430.2025.2483474>

Link to Leeds Beckett Repository record:

<https://eprints.leedsbeckett.ac.uk/id/eprint/12095/>

Document Version:

Article (Published Version)

Creative Commons: Attribution 4.0

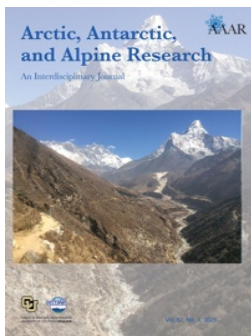
© 2025 The Author(s)

The aim of the Leeds Beckett Repository is to provide open access to our research, as required by funder policies and permitted by publishers and copyright law.

The Leeds Beckett repository holds a wide range of publications, each of which has been checked for copyright and the relevant embargo period has been applied by the Research Services team.

We operate on a standard take-down policy. If you are the author or publisher of an output and you would like it removed from the repository, please [contact us](#) and we will investigate on a case-by-case basis.

Each thesis in the repository has been cleared where necessary by the author for third party copyright. If you would like a thesis to be removed from the repository or believe there is an issue with copyright, please contact us on openaccess@leedsbeckett.ac.uk and we will investigate on a case-by-case basis.



Arctic, Antarctic, and Alpine Research

An Interdisciplinary Journal

ISSN: 1523-0430 (Print) 1938-4246 (Online) Journal homepage: www.tandfonline.com/journals/uaar20

Land cover change across the major proglacial regions of the sub-Antarctic islands, Antarctic Peninsula, and McMurdo Dry Valleys, during the 21st century

Christopher D. Stringer, Jonathan L. Carrivick, Duncan J. Quincey, Daniel Nývlt & Alexis Comber

To cite this article: Christopher D. Stringer, Jonathan L. Carrivick, Duncan J. Quincey, Daniel Nývlt & Alexis Comber (2025) Land cover change across the major proglacial regions of the sub-Antarctic islands, Antarctic Peninsula, and McMurdo Dry Valleys, during the 21st century, Arctic, Antarctic, and Alpine Research, 57:1, 2483474, DOI: [10.1080/15230430.2025.2483474](https://doi.org/10.1080/15230430.2025.2483474)

To link to this article: <https://doi.org/10.1080/15230430.2025.2483474>



© 2025 The Author(s). Published with license by Taylor & Francis Group, LLC.



[View supplementary material](#)



Published online: 07 May 2025.



[Submit your article to this journal](#)



Article views: 150



[View related articles](#)



[View Crossmark data](#)



Land cover change across the major proglacial regions of the sub-Antarctic islands, Antarctic Peninsula, and McMurdo Dry Valleys, during the 21st century

Christopher D. Stringer ^{a,b}, Jonathan L. Carrivick ^b, Duncan J. Quincey ^b, Daniel Nývlt ^c,
and Alexis Comber ^b

^aSchool of Built Environment, Engineering and Computing, Leeds Beckett University, Leeds, UK; ^bSchool of Geography and Water, University of Leeds, Leeds, UK; ^cPolar-Geo-Lab, Department of Geography, Faculty of Science, Masaryk University, Brno, Czech Republic

ABSTRACT

Land cover information is essential for understanding Earth surface processes and ecosystems. Here, we use *K*-means clustering to classify Landsat 8 Operational Land Imager (OLI) images covering six proglacial sites of sub-Antarctic islands, the Antarctic Peninsula, and the McMurdo Dry Valleys at 30-m resolution. We quantify spatial patterns of water, bedrock, vegetation, and sediments to an accuracy of 77 percent. Vegetation is most abundant on South Georgia (7 percent of the proglacial area) and the South Shetland Islands (1 to 2 percent). Furthermore, we use change vector analysis (CVA) to discriminate landcover change in the twenty-first century. A latitudinal pattern is evident in ice loss and proglacial landscape change; for example, loss of ice on South Georgia and proglacial landcover change is two orders of magnitude greater than in the McMurdo Dry Valleys. Four of the studied sites had similar landscape stability (64 to 68 percent unchanged), with Alexander Island an exception (50 percent change) due to recent enhanced glacier melt. Overall, we show how landcover of proglacial regions of the climatically sensitive sub-Antarctic and Antarctica has changed since 2000, with a CVA accuracy of 80 percent. These findings inform understanding of geomorphological activity and sediment and nutrient fluxes and hence terrestrial and marine ecosystems.

ARTICLE HISTORY

Received 22 February 2024
Revised 7 March 2025
Accepted 13 March 2025

KEYWORDS



Antarctica; proglacial; LULC; land cover; sediment


Introduction

Consistent land cover information is essential to furthering our understanding of terrestrial environments, ecological niches, and the atmosphere, especially across sensitive regions of Earth (Raup et al. 2007; Ban, Gong, and Giri 2015; Chen, Li, and Wang 2019; Gong et al. 2020). Additionally, land cover maps are a critical resource required to support the research of climate change, particularly those that include information on vegetation coverage (Bojinski et al. 2014). Different types of land cover can change or respond to climatic forcing in different ways, depending on their physical and chemical properties (GCOS 2010). Owing to the frequent return period and extensive areas covered by satellite images, land cover maps are increasingly being produced using remote sensing techniques and the changes occurring in the landscape can thus be detected and quantified (Friedl et al. 2010; Lea 2018; Brown et al. 2022). Several global land cover products

have been released in recent years (e.g., Brown et al. 2022), but they typically do not include Antarctica or sub-Antarctic Islands (e.g., South Georgia), leaving a gap in our understanding of Earth's southernmost continent.

The majority (99.8 percent) of Antarctica is covered by ice, with the remaining 0.2 percent characterized as nunataks (i.e., mountain peaks that penetrate the ice sheet) or as proglacial regions (Burton-Johnson et al. 2016; Figure 1). Proglacial regions are predominantly shaped by the interplay of meltwater from glaciers, which erodes, transports, and deposits sediment, and hillslope activity, which largely acts to supply new sediment into the system during mass transport events. In a warming climate, the activity of water and increased mass movements result in greater sediment discharge (Ballantyne 2008; Klaar et al. 2015; Staines et al. 2015). In polar regions, where permafrost can be extensive, the active layer is an additional and important water and

CONTACT Christopher D. Stringer  C.D.Stringer@leedsbeckett.ac.uk  School of Built Environment, Engineering and Computing, Leeds Beckett University, Northern Terrace, Queen Square Ct., Leeds LS2 8NU, UK.

 Supplemental data for this article can be accessed online at <https://doi.org/10.1080/15230430.2025.2483474>.

© 2025 The Author(s). Published with license by Taylor & Francis Group, LLC.

This is an Open Access article distributed under the terms of the Creative Commons Attribution License (<http://creativecommons.org/licenses/by/4.0/>), which permits unrestricted use, distribution, and reproduction in any medium, provided the original work is properly cited. The terms on which this article has been published allow the posting of the Accepted Manuscript in a repository by the author(s) or with their consent.

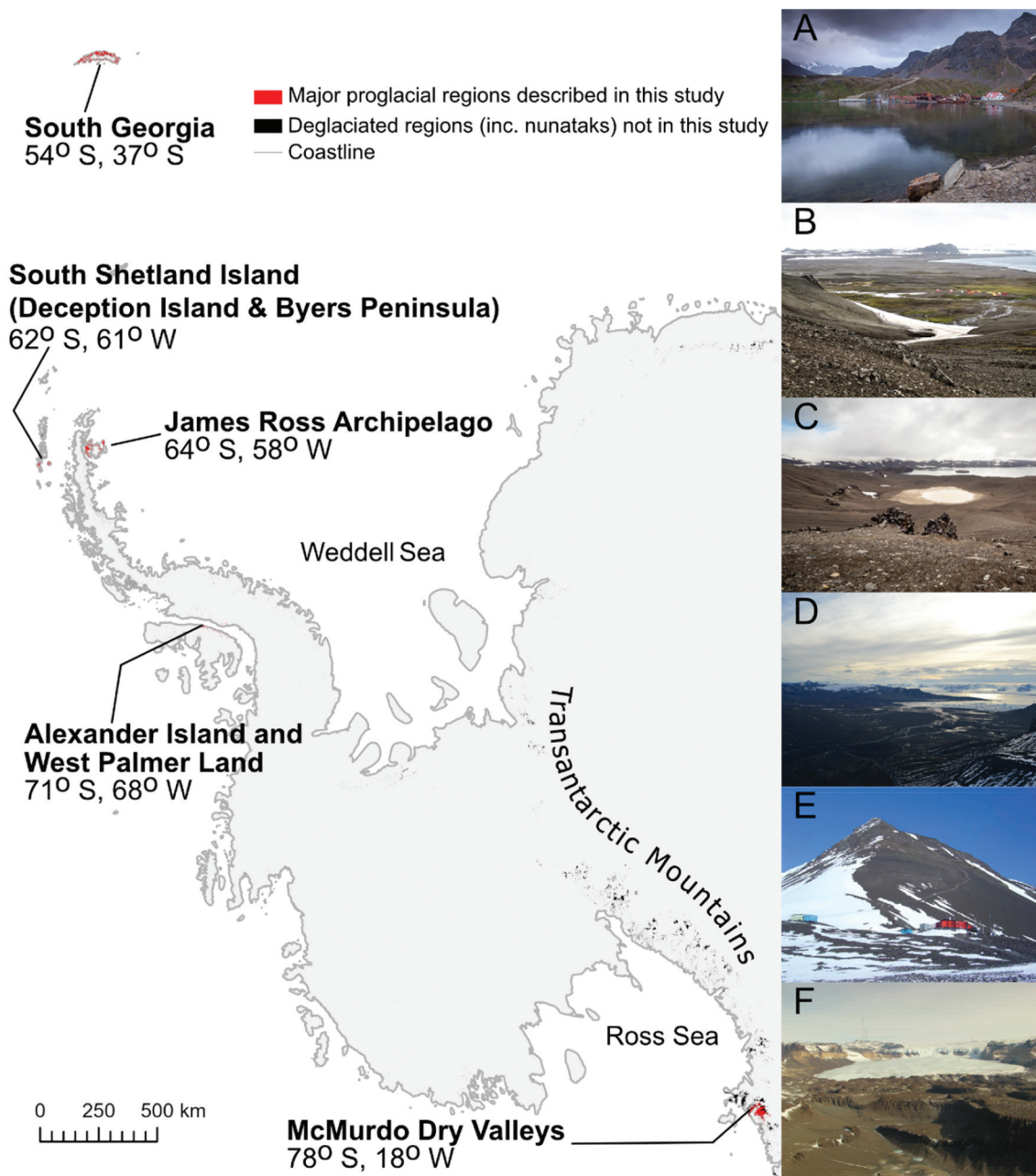


Figure 1. Location of our study sites. The areas analyzed are highlighted in red and span a latitudinal gradient from 54° S to 78° S. Proglacial regions not analyzed in this study are highlighted in black (Burton-Johnson et al. 2016) and are primarily mountains (e.g., Transantarctic Mountains) or are frequently covered by extensive cloud cover (e.g., King George Island). (A) Grytviken on South Georgia. Taken in 2009 by Simon Murgatroyd (CC BY-SA 2.0). (B) Camp Byers on South Beach (ESP) on Byers Peninsula. Taken in 2017 by “Inoceramid bivalves” (CC BY-SA 4.0). (C) Telefon Bay (background), as viewed from the rim of a crater on Deception Island. Taken in 2020 by Espen Mills (CC BY-SA 4.0). (D) Abernethy Flats on James Ross Island’s Ulu Peninsula, as viewed from Lachman Crags, above Triangular Glacier (looking West), taken in 2022. (E) The central station of Fossil Bluff on Alexander Island in 2003. Photo taken in 2003 by “Apacheeng lead” (Public Domain). (F) The Wright Valley of the McMurdo Dry Valleys (looking west toward Wright Upper Glacier) in 2013, taken by “Turkish D.” (CC BY-SA 4.0). Inset photos (A), (B), (D), (E), and (F) were sourced from Wikimedia Commons. Photo (C) by Christopher D. Stringer.

sediment source on days when ground temperatures exceed 0°C (Humlum, Instanes, and Sollid 2003; Kavan et al. 2017; Costa et al. 2018; Łepkowska and Stachnik 2018). All of these factors mean that the Antarctic landscape is highly dynamic.

Maps of land cover and land cover change are particularly important for Antarctica, owing to its dynamic landscape and rapid environmental change (Davies et al. 2013). Unlike most other regions on Earth, human activities are not the major control on land cover type

in Antarctica, and the footprint of anthropogenic activities is limited to relatively small areas (Tejedo et al. 2016, 2022). Until the start of the twenty-first century, the Antarctic Peninsula Region (APR) was one of the most rapidly warming places on Earth, with a temperature rise of 1.5°C observed since the 1950s (Vaughan et al. 2003; Mulvaney et al. 2012; Oliva et al. 2017). Following a hiatus in warming at the start of the twenty-first century, there is evidence that this trend has resumed (Carrasco, Bozkurt, and Cordero 2021) and glaciers have continued to respond to the temperature increases of the twentieth century and subsequent warming since 2015 (Oliva et al. 2017; Engel et al. 2023). Consequently, glacier mass loss has occurred at an enhanced rate, particularly around smaller ice masses in the APR and sub-Antarctic islands (Oliva et al. 2017; Engel et al. 2018; Rosa et al. 2020). This ice mass loss has resulted in the enlargement of proglacial regions, and they will continue to expand as both land- and marine-terminating glaciers continue to retreat with a warming climate (Nedbalová et al. 2013; Lee et al. 2017; Roman et al. 2019).

In this study we will map the land cover of six major proglacial regions in Antarctica: (1) South Georgia, (2) southern Livingston Island and Snow Island (hereafter referred to as Byers Peninsula), (3) Deception Island, (4) James Ross Archipelago, (5) Alexander Island, and (6) the McMurdo Dry Valleys (Figure 1). These sites are conspicuous for their lack of consistent land cover data between the sites. Though geological and geomorphological studies have produced maps at the sites (e.g., Table 1), they lack a common nomenclature. Similarly, many of these maps are several decades old or no map of their surface exists. On Alexander Island, for example, very few descriptions of the landscape or land cover are available, with limited descriptive accounts (Heywood, Fuchs, and Laws 1977) and only very limited geomorphology maps of the region available (M. C. Salvatore 2001). In contrast, some regions have been the subject

of extensive mapping studies. James Ross Island, for example, has been home to several geological and geomorphological surveys, though these studies are either limited to the Ulu Peninsula (Davies et al. 2012; Mlčoch, Nývlt, and Mixa 2020; Jennings et al. 2021) or lack detail on land cover information beyond the geology (Smellie 2013). Though there have been recent, substantial, efforts in improving the understanding of vegetation extent in Antarctica (Walshaw et al. 2024), there continues to be a lack of understanding of other important land features.

Understanding the makeup of Antarctica's proglacial regions and how those land surface components are changing is important because they are a source of water, sediment, and solutes. The quantity and spatiotemporal pattern of sediment discharged from Antarctica have profound effects on the ecosystem of the Southern Ocean and polar lakes, which in turn can affect the rate at which carbon is sequestered from the atmosphere (Brussaard et al. 2008; Maat, Visser, and Brussaard 2019). Additionally, changes in vegetation cover can have wide-ranging impacts on wildlife. In a warming climate, the natural range of indigenous species may increase (Convey and Smith 2007). Similarly, people visiting the APR and sub-Antarctic may introduce invasive species (Galera et al. 2021; Tejedo et al. 2022). The establishment of invasive species can expand the vegetated area, displace indigenous biota, increase competition, and alter food web linkages, potentially threatening the survival of indigenous species (Molina-Montenegro et al. 2012; Hughes et al. 2020). It is therefore important to have a baseline data set that describes the land cover composition of proglacial landscapes (Carrivick et al. 2018, 2019) so that future changes may be quantified. Furthermore, understanding how proglacial landscapes have responded to recent ecological and climatic change is useful for understanding how these systems may evolve in the future (Wilkes et al. 2023).

Table 1. Resources used to interpret clusters and assign them to a land class.

Location	Resources
James Ross Island	Geomorphology map, Jennings et al. (2021) Geomorphology map, Davies et al. (2013) Geological map, British Antarctic Survey, Smellie (2013) Geological map, Czech Geological Survey, Mlčoch, Nývlt, and Mixa (2020) Vegetation map, Barták et al. (2015)
Dry Valleys	Interactive geological map, SCAR, Cox et al. (2023)
Alexander Island	Geological map, British Antarctic Survey (1981)
Deception Island	Geology and geomorphology map, British Antarctic Survey, Smellie et al. (2002) ASPA 140 (map of vegetation), Secretariat of the Antarctic Treaty (2022)
Livingston Island	Geomorphology map, Lopez-Martinez et al. (1996) Vegetation map, Ruiz-Fernández et al. (2017)
South Georgia	Geomorphology map, Clapperton (1971)

The aims of this article are to (1) produce the first unified map of land cover across the major proglacial areas of APR, sub-Antarctic, and the Dry Valleys; (2) quantify the overall accuracy of our data and how that accuracy varies spatially; and (3) identify regions that have changed during the twenty-first century.

Study sites

There is a dearth of literature that seeks to characterize proglacial regions, particularly in Antarctica. Some research has been conducted on individual rivers and catchments, notably on the Onyx River (Chinn and Mason 2016), James Ross Island's Ulu Peninsula (Davies et al. 2013; Nedbalová et al. 2013; Kavan et al. 2017; Jennings et al. 2021; Kavan 2021; Sroková and Nývlt 2021), and other sub-Antarctic islands, such as the South Shetland Islands (Mink et al. 2014; Oliva et al. 2016). However, these studies have taken varying approaches to characterizing landscape compositions, and there is little in the way of a consistent land cover data set of these proglacial regions. Additionally, important global data sets fail to characterize the land cover of Antarctica (e.g., Brown et al. 2022).

Climate

All six study sites have polar climates but span both maritime and continental settings. The sites are positioned along a latitudinal gradient and so permit an analysis of land cover variability with climatic patterns. The most northern site, South Georgia, is characterized by its high relief and has a mean annual air temperature (MAAT) of 3°C, as well as receiving over 2,000 mm of precipitation per year (Bannister and King 2015; Strother et al. 2015). Over half of South Georgia is glacierized (Bannister and King 2015). The South Shetland Islands are characterized by a polar maritime climate, with air temperatures regularly exceeding 0°C in summer. The humid environment, due to its maritime location, ice-free seas, and regular cyclonic activity, results in liquid precipitation falling regularly in the summer months (Bañón et al. 2013). The James Ross Archipelago, to the northeast of the Antarctic Peninsula, has an MAAT of −7°C and has a semi-arid polar continental climate (Kaplan Pastíriková et al. 2023). The two more southerly sites, Alexander Island and the McMurdo Dry Valleys, have continental climates (Harangozo, Colwell, and King 1997). Alexander Island, specifically Fossil Bluff, has an MAAT of −9°C and receives approximately 200 mm of precipitation each year (Harangozo, Colwell, and King 1997; Davies et al. 2017). The McMurdo Dry Valleys are distinctly colder and drier than the other sites; they are hyper-arid

due to katabatic winds and have an MAAT of −17°C to −20°C (Doran, Wharton, and Lyons 1994; Marchant and Head 2007).

Methodology

Site selection

Our site selection was informed by the British Antarctic Survey's rock outcrop data sets (Burton-Johnson et al. 2016; Gerrish, Fretwell, and Cooper 2020), allowing us to focus primarily on the nonglacierized landscape. Nunataks in the interior of the ice sheets were excluded because they were too small to classify at 30-m resolution, and we could assume their classification to be bedrock. Because they are disconnected from the coastline, they can also be assumed largely unimportant as sediment sources to the Southern Ocean. Fossil Bluff and other coastal regions on Alexander Island and Palmer Land were included and are interesting for their proximity to George VI Sound. These regions may become important sediment sources in the near future, because exceptional melting in this region appears to have increased the likelihood of the George VI ice shelf collapsing (Banwell et al. 2021). We further narrowed the site choices to consider only those regions with cloud-free Landsat 8 Operational Land Imager (OLI) images.

Land cover classifications

In the last decade, satellite data from the Landsat and Sentinel programs have become open source and increasingly easy to access. In tandem with improved computational power, such as that provided by cloud-based platforms like Google Earth Engine (GEE), it is now possible to produce land cover maps at a medium spatial resolution (10–30 m) using openly available data. The Landsat 8 satellite also has the benefit of being part of a continuation program, making interdecadal comparison possible.

Image selection and pre-processing

We classified Landsat 8 OLI (top-of-atmosphere) images acquired between 2016 and 2020 (see Supplementary Material Section 1.6 for details) in GEE and ESRI ArcGIS Pro 2.6.0, primarily using K-means clustering (using GEE's default settings, including ten randomized seeds). Though we have chosen to use GEE and ArcGIS Pro 2.6.0 for this research, it would be functionally possible to repeat our methodology using other software. We chose Landsat imagery, rather than higher-resolution images (such as Sentinel-2), because of its extensive archive dating back to 1972. Suitable images

had low cloud cover (less than 20 percent over land) and limited snow cover. Images were cloud masked (using Landsat's quality assessment band) and, where more than one image was available, we mosaicked them, taking the least cloudy/snowy scene as the uppermost image, thus minimizing the snow and cloud cover across the unified scene.

To ensure consistency with older Landsat images, we only selected six bands representing the visible and infrared wavelengths (red, green, blue, near-infrared, shortwave infrared 1, and shortwave infrared 2, ranging from 0.45 to 2.29 μm) from the images for classification. We added three further bands to the image in the form of the Normalized Difference Snow Index (NDSI; Equation (1)), the Normalized Difference Vegetation Index (NDVI; Equation (2)), and the Normalized Difference Water Index (NDWI; Equation (3)). These aided the classifier in the identification of key land cover classes (ice, vegetation, and water, respectively).

$$NDSI = \frac{\text{green} - \text{swir1}}{\text{green} + \text{swir1}} \quad (1)$$

$$NDVI = \frac{\text{nir} - \text{red}}{\text{nir} + \text{red}} \quad (2)$$

$$NDWI = \frac{\text{green} - \text{nir}}{\text{green} + \text{nir}} \quad (3)$$

where

- green = band 3 of Landsat 8 OLI, wavelength (λ) = 0.53 to 0.59 μm
- swir1 = shortwave infrared 1, band 6, λ = 1.57 to 1.65 μm
- red = band 4, λ = 0.64 to 0.67 μm
- nir = near-infrared, band 5, λ = 0.85 to 0.88 μm

We clipped the images to a 1-km buffer around their coastline (Gerrish, Fretwell, and Cooper 2021) and topographically corrected them to adjust for the effect of relief on the illumination of images using the Sun Canopy Sensor + C method (Soenen, Peddle, and Coburn 2005) with the Reference Elevation Model of Antarctica mosaic digital surface model (Howat et al. 2019) at 30-m resolution (equivalent to the resolution of Landsat 8 OLI multispectral bands). South Georgia, which is not covered by Reference Elevation Model of Antarctica, was corrected using the Shuttle Radar Topography Mission Digital Elevation Model, also at 30-m resolution (Farr et al. 2007). Subsequently, we conducted a principal component analysis of the images, and the first three components, containing 99.6 percent (± 0.3 percent) of the data, were selected for classification (Frohn et al. 2009; Chasmer et al. 2020).

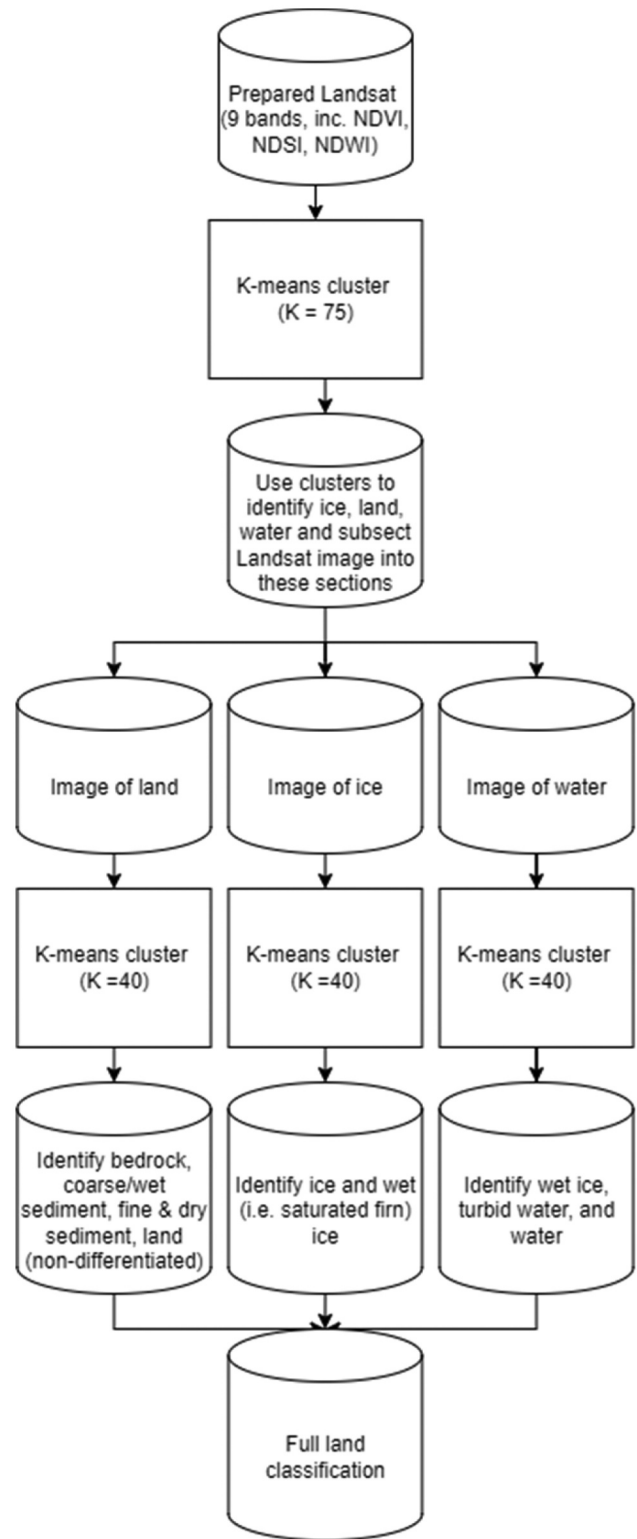


Figure 2. Our approach to classifying land cover.

Classification

We used a hierarchical *K*-means clustering approach to classify Landsat 8 OLI images (Figure 2). *K*-means is widely used in land classification studies (Phiri and

Morgenroth 2017; Grimes et al. 2024) and is preferential to over other unsupervised approaches (e.g., ISODATA) because it can be used to identify a user-defined number of classes. *K*-means works by segmenting an image into distinct clusters, which the user then interprets to classify these clusters using existing knowledge of the field or previously published maps often based on field research (e.g., Table 1). A first-order land classification (clustered with $K = 75$, see Supplementary Material Section 1.1) of “land,” “snow and ice” (hereafter referred to simply as “ice”), and “water” informed the subdivision of each of these classes in a second, more detailed, analysis of the dominant land cover classes (further details in Supplementary Material Section 1.2.). A two-stage approach was used to limit misclassification by ensuring that water, ice, and bare land were in distinct classes. The code used to produce this classification is also publicly available (see section 2.4.5).

We used this first-order land classification to subset each image accordingly and then to cluster these resulting images into forty discrete groups ($K = 40$). Specific *K* values were determined through expert judgment and represent values that minimized the chance of misclassification (see further details in Supplementary Material 1.1). Using the limited catalog of published maps and literature available for these areas (see Table 1), we visually inspected these clusters to manually assign each of them a final land classification. Our first-order land class was subset into five classes: “bedrock,” “coarse/wet sediment,” “fine & dry sediment,” “vegetation,” and “land (nondifferentiated).” The water class was subset into “water” and “turbid water,” and the ice class was subset into “ice” and “wet ice.” In cases where clouds partially obscured land, we assigned pixels to the more general class of “land (nondifferentiated).” Therefore, we produced ten land classes that describe eight distinct surface types (plus no data and land undifferentiated; see Supplementary Material for more details) that could be identified from a combination of field observations and a review of available maps of Antarctica (Table 1) and finding commonalities between them (further details in Supplementary Material Section 1.3.).

During the classification process, we created two different sedimentary classes because we found that pixels containing wet sediments (such as rivers) or blocky superficial sediments, such as scree, clustered distinctly from those pixels that contain sediments smaller than cobbles in size and fissile sedimentary rocks. This approximate grain size threshold was derived from information on geomorphological maps for the region (Jennings et al. 2021) and observations made on James Ross Island during the 2022 field season. We emphasize

that the first of these two classes describe pixels that contain sediment that may be coarse, wet, or both. The second of these classes describes surfaces with fine sediments with minimal water content.

Accuracy assessment

Having used the limited preexisting maps and field survey data to inform our interpretation of the *K*-means clusters, we had to depend on finer-resolution imagery as the primary independent validation source, with interpretation of images aided by the use of previously published maps. Although we could not find alternative land cover data, we still used the methods of best practice described by Olofsson et al. (2013, 2014) to that ensure our accuracy assessment was robust (see Supplementary Material Section 1.5). Therefore, we generated 3,000 random points, stratified by the area of each land class, and visually compared them to 10-m resolution Sentinel-2 MultiSpectral Instrument images. Sentinel-2 MultiSpectral Instrument images were used as an independent data source for validation because they are finer resolution than Landsat images, thus giving a better indication of the “true” land cover. Given the dominance of the ice class in our classification, this meant that most of the stratified sample points landed on ice. We conducted a second level of accuracy assessment with 1,000 points on just the proglacial classes to ensure that their accuracy was adequately calculated.

The classes of turbid water and wet ice were particularly problematic because they typically comprised episodic sediment plumes and snow/ice melt. Therefore, we combined these classes with water and ice respectively for the purposes of accuracy assessment. We produced a 10-km-resolution grid to display the spatial variability in the accuracy of this classification (as a proxy for confidence), with each cell color-coded according to the percentage of accurate assessment points within it. Full accuracy assessment matrices are available in the supplementary material (Section 1.5).

We also compared the spectra for each land type to ensure that each land type could reasonably be differentiated from the others.

Change detection

We repeated the search described in section 2.2.2 for Landsat 7 Enhanced Thematic Mapper Plus (ETM+) images acquired for each of our sites between 2000 and 2003 and conducted change detection (Figure 3). This search resulted in a pair of image mosaics (hereafter referred to as image pairs) for five sites, comprising a mosaic from the early 2000s (Landsat 7) and

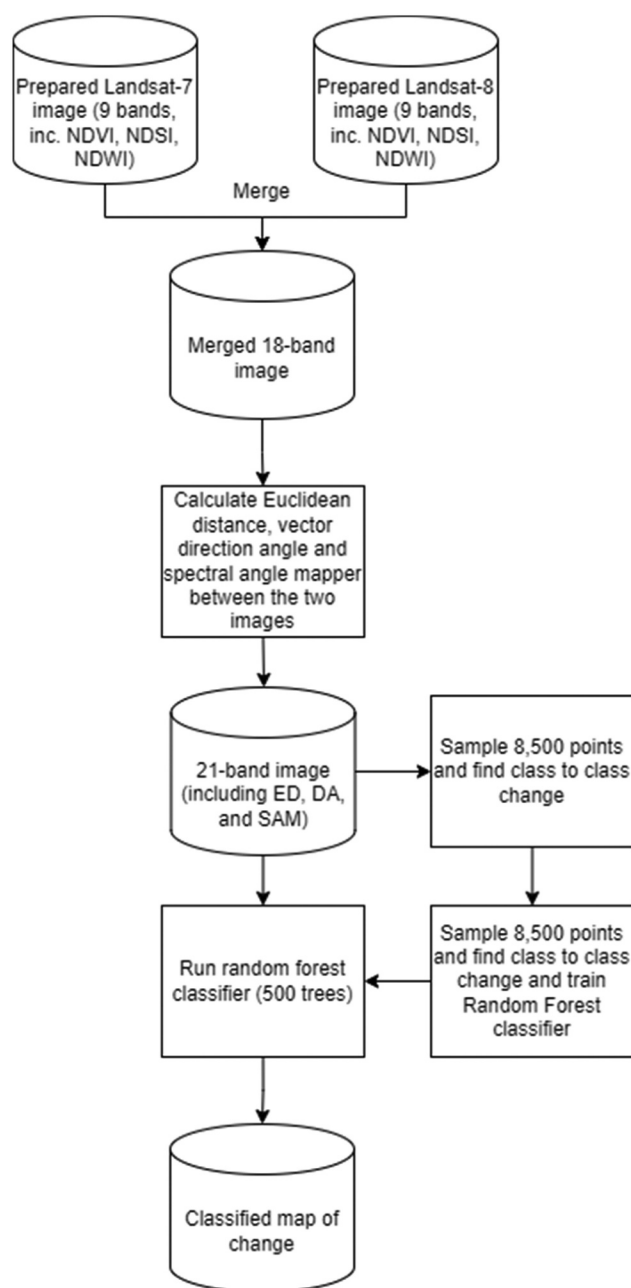


Figure 3. The change detection (CVA) approach used in this study.

a mosaic from close to 2020 (Landsat 8). It was not possible to find a suitable image for Deception Island, so we could not conduct change detection for this site; this meant that change detection was conducted over only five of the six sites for which a land cover map was produced. We manually inspected the image pairs for each site to ensure that they were co-registered using geographic information systems. We aimed to ensure that both mosaics comprised images collected from the same time of year to ensure that they represented the same part of the growth and hydrological season and avoided images with high snow cover, where possible. In

some cases, poor image availability meant that some image pairs could not be collected from the same time of year (though the temporal difference was minimized). We ensured that key features such as flowing rivers and unfrozen lakes were, as much as possible, present in both mosaics. Then we conducted a change vector analysis (CVA) to identify regions of change in each of our sites using the approach described by (Xu et al. 2018). Further details of the CVA approach used can be found in the supplementary material (Section 1.4).

Accuracy assessment

To validate the accuracy of our change maps, we reproduced the change detection analysis on Byers Peninsula with a 70:30 split of the training points between the classifier and validation. This approach is regularly used to assess the accuracy of land cover and change products, in the absence of independent data (Xu et al. 2018), and this ratio between training and validation has been shown to be most reliable (Adelabu, Mutanga, and Adam 2015). By splitting the data 70:30 between training and validation, the 30 percent of pixels used for validation are “independent” of those used by the classifier. To ensure that this split was unbiased, we randomly sorted the training points.

Results and interpretations

Land cover classifications

The land classes

The largest land class at our sites is ice; the large ice sheets and glaciers at all sites have been mapped, though this class also includes limited snow cover. Though mapping ice masses is not the primary goal of this study, the high accuracy (see section 3.3.1) of the ice class makes this data set a useful resource to assess changes in the small land-terminating glaciers within our study sites (Figure 4).

Of the sedimentary classes, coarse and wet sediment is the predominant land class at four of the six sites, particularly on South Georgia and Byers Peninsula, where it represents the majority (57 and 56 percent, respectively) of the proglacial land cover (Figures 5 and 6). This land class includes the major surface drainage networks of Antarctica (Figure 4); for example, it accurately depicts the major rivers of the Bohemian Stream and Abernethy River on James Ross Island and the Onyx River in the McMurdo Dry Valleys (cf. Chinn and Mason 2016; Kavan et al. 2017; Jennings et al. 2021). The coverage of fine and dry sediment class varies inversely to that of the coarse/wet sediment. For example, on South Georgia, the 57 percent coverage of coarse

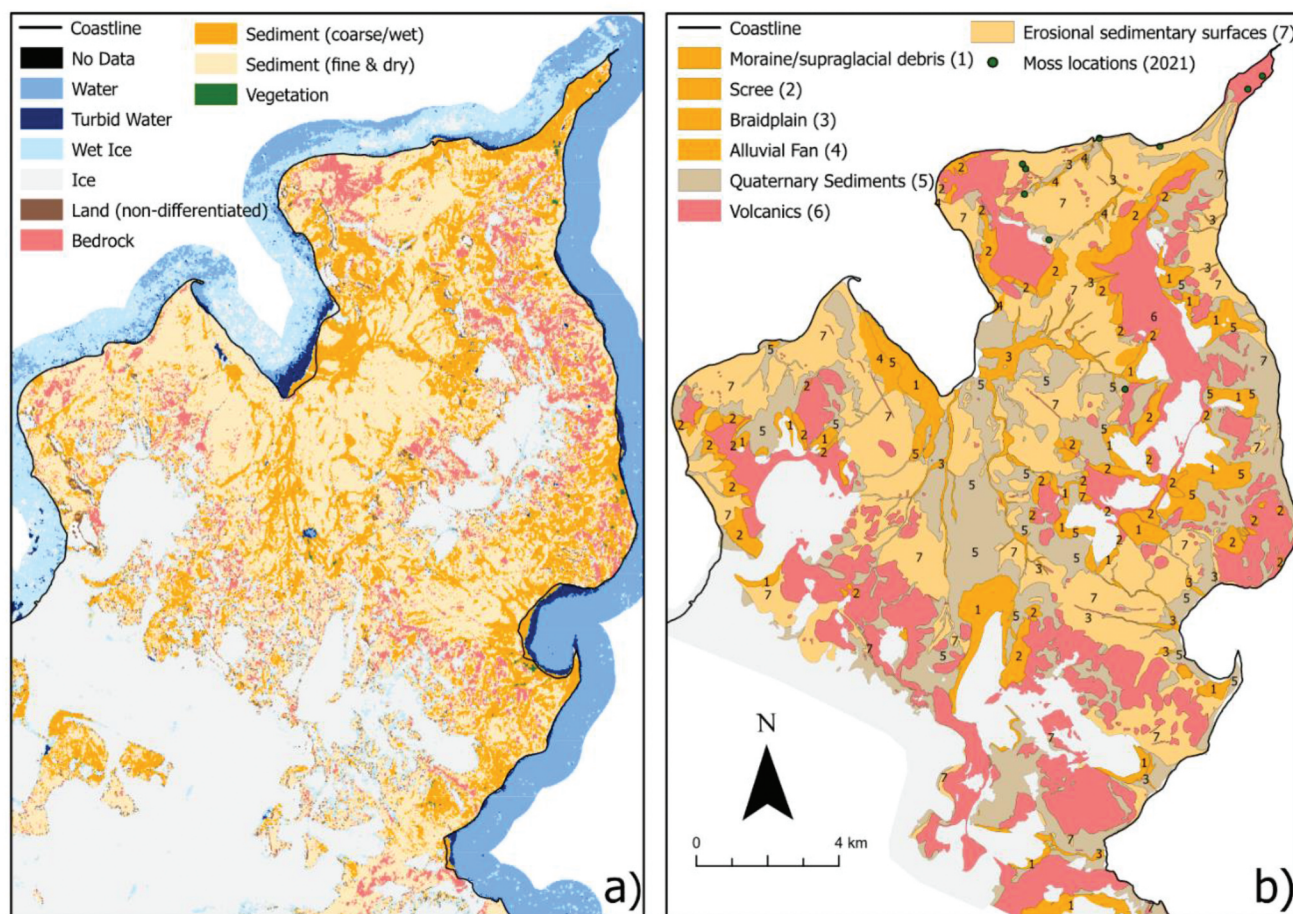


Figure 4. A comparison between (a) the land classification produced in this study and (b) a geomorphology map, adapted from Jennings et al. (2021). Jennings et al. (2021) produced these data through a series of extensive field surveys on the Ulu Peninsula. Vegetation locations as collected in the field by Jan Kavan (of the Czech Antarctic Research Programme) in 2021 are also displayed. Note the similarities in the ice class, locations of river systems, and scree slopes. The colors in (b) have been adapted to allow a more direct comparison with the map produced in this study (a).

sediment is in comparison to a 33 percent coverage of fine and dry sediment. On Deception Island, where fine and dry sediments are the dominant land class (53 percent), there is only 26 percent coverage of coarse/wet sediment (Figure 6). At all of the sites, between 70 and 80 percent of the proglacial surface is covered by sediment. The bedrock class, which primarily describes igneous and metamorphic rock surfaces, is most abundant on Deception Island, comprising 14 percent of its proglacial areas (Figure 6). It is of similar abundance in the Dry Valleys (13 percent), with between 7 and 9 percent of Alexander Island, James Ross Archipelago, and Byers Peninsula comprising bedrock. The absence of the bedrock class on South Georgia is accounted for by its lack of igneous outcrops, as well as well-developed sedimentary systems and extensive vegetation cover (Clapperton 1971).

The classes relating to water (water, turbid water, wet ice) are of varying quantities across all of the sites and

may represent transient features (e.g., seasonal melt-water/sediment plumes). The wet ice class proved to be a little ambiguous to interpret from clusters and represents saturated firn and “slush” ice (i.e., partially melted ice or partially frozen water). Wet ice is most abundant on Alexander Island, with 17 percent coverage (Figure 6), and highlights the record-high surface melt observed around the King George VI Ice Shelf in late 2019 (Banwell et al. 2021). This large amount of wet ice is comparable to the James Ross Archipelago (15 percent), where a large proportion of wet ice is accounted for by a melt event that resulted in a large area of saturated firn on Snow Hill Island (Figure 7). This transient nature of wet ice is also seen with the turbid water class, which can pick out sediment plumes (Figure 7).

Our land classification has also identified regions of vegetation. This includes extensive areas of vegetation on South Georgia, which we have calculated to cover 8 percent of its proglacial surface and are clearly identifiable in

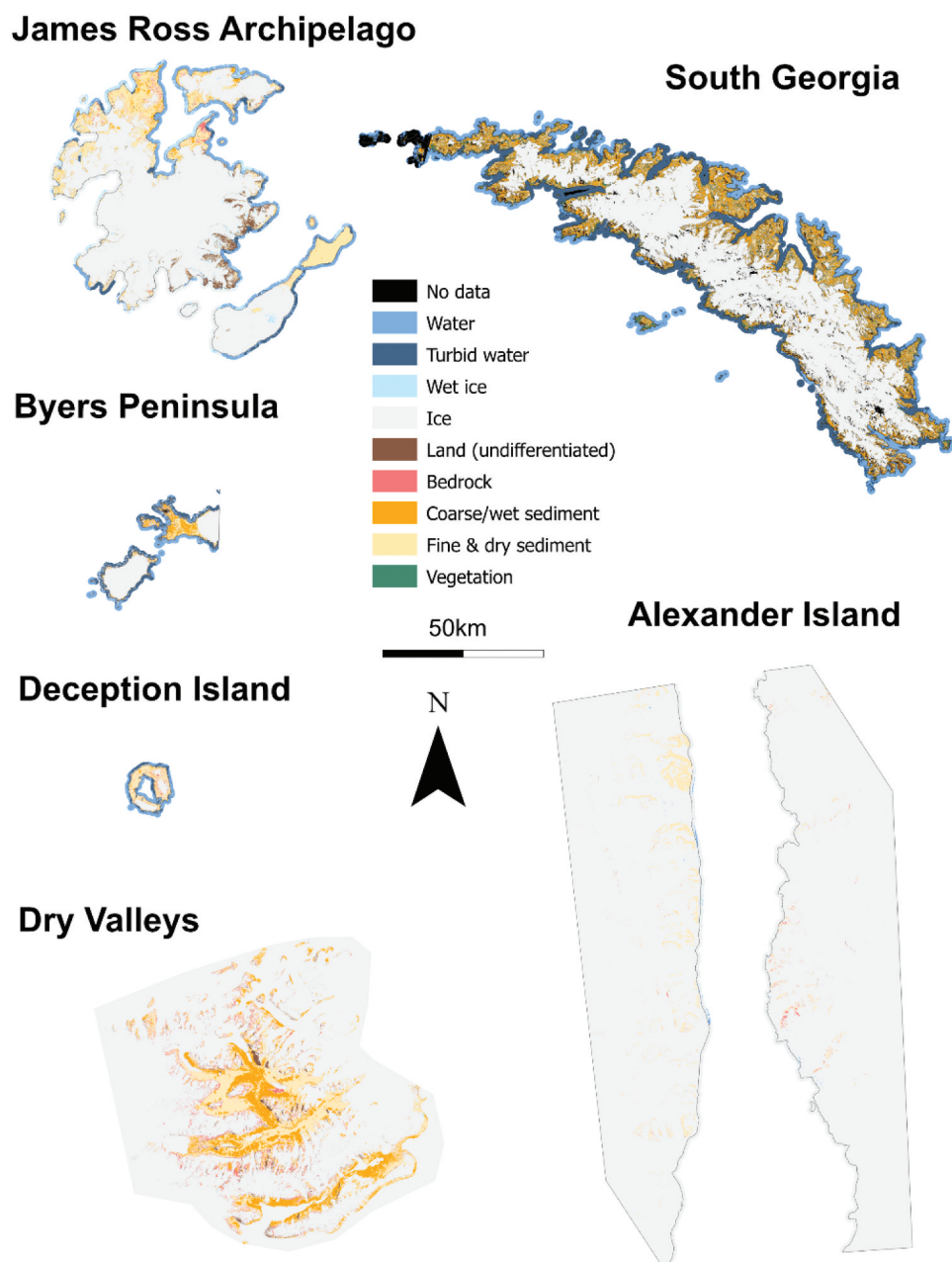


Figure 5. Land cover maps of the six sites, including ten classes that describe eight distinct surfaces. Ice class may include limited areas of seasonal snow cover. Higher resolution maps can be found in the supplementary material (Section 2).

satellite images (Figure 6). We have also identified several sites of vegetation on the South Shetland Islands; especially those on Deception Island (total 1 percent surface coverage; Figure 6) within ASPA 140 (subsite B) on Deception Island (Secretariat of the Antarctic Treaty 2022). In some cases, we have even been able to identify very small areas of vegetation such as those located on James Ross Island, which were verified in the field (Figure 4).

Spatial variations

We observe a spatial variation in land cover between the sites (Figures 5 and 6). There is typically more coarse/wet sediment at sites further away from the pole; this is offset by a general decrease in fine and dry sediments. However, the Dry Valleys are an exception to this, with 44 percent of the land covered by coarse or wet sediments. The second most southern site, Alexander Island,

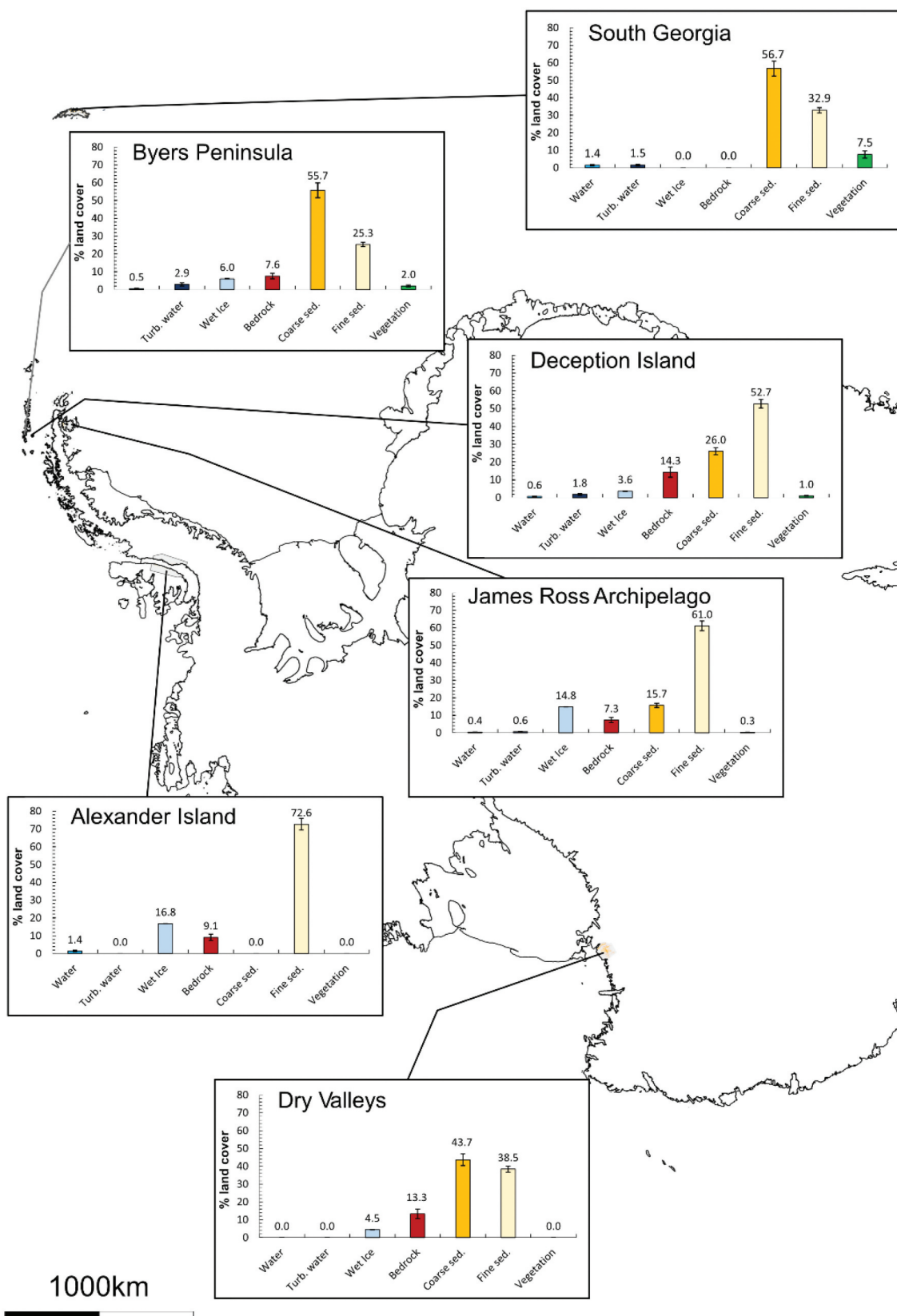


Figure 6. Percentage land cover values (excluding ice, no data, and land [undifferentiated]) for each site, overlaying the coastline of Antarctica (coastline sourced from BAS). Error bars indicate the 95 percent confidence intervals.

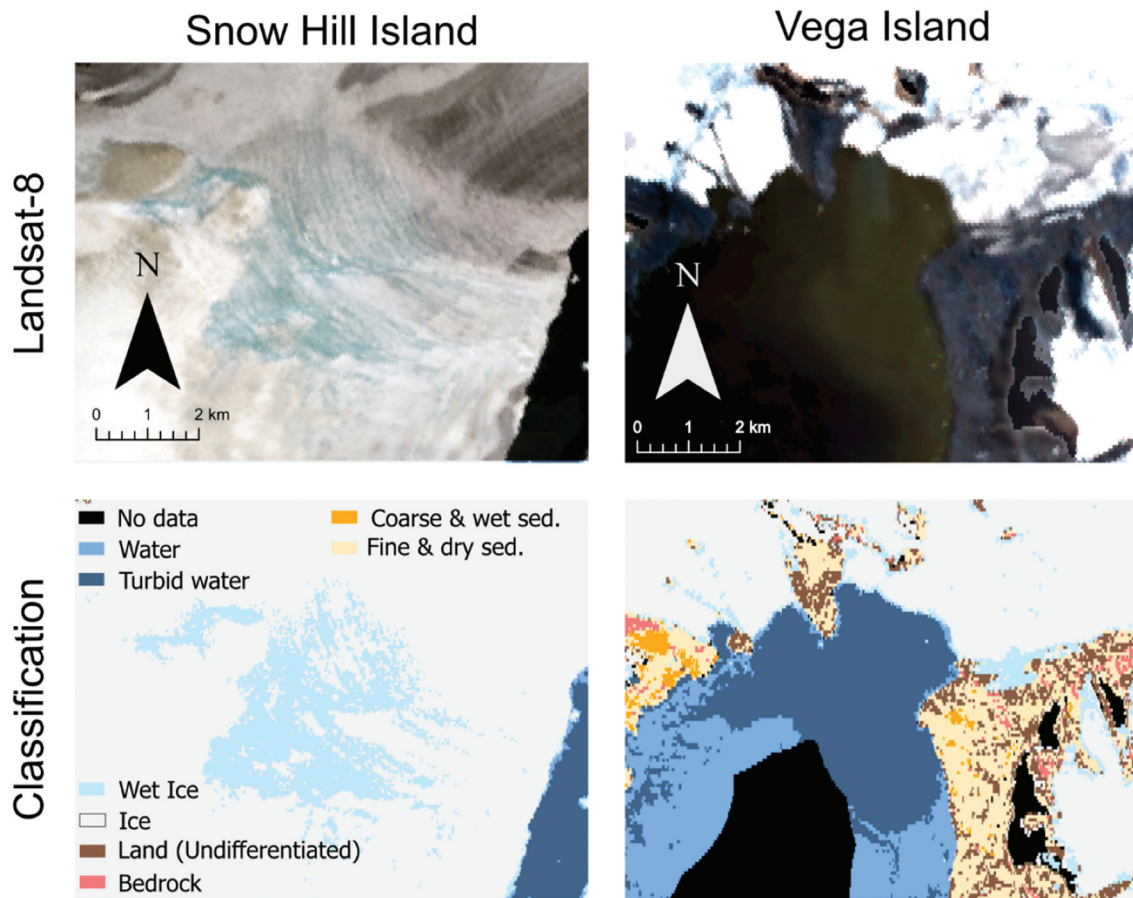


Figure 7. How the wet ice and turbid water classes compare to the images they are derived from, with a large area of saturated firn on Snow Hill Island (64°28' S, 57°4' W) and a sediment plume off the coast of Vega Island (63°52' S, 57°16' W).

has 0 percent of its proglacial surface covered by coarse/wet sediment, compared with 57 percent on South Georgia.

Unlike other land classes, the proportion of the (inland) water and wet ice classes appears to be more evenly spread across the sites. There is a slight apparent latitudinal pattern in these data, with more water at the sites further to the north and variability between the east and west (i.e., when comparing the South Shetland Islands with James Ross Archipelago; [Figure 6](#)). South Georgia and Byers Peninsula have the largest amount of liquid water present (when joining the water and turbid water classes together), around 3 percent. James Ross Archipelago has significantly less (1 percent), and 1 percent of Alexander Island's surfaces is classified as water, owing to a large amount of supraglacial water at the time of image acquisition. We classified some of this melt as water, rather than wet ice, because it was unambiguously liquid when we inspected and interpreted the clusters. Much of these intersite differences in liquid water likely represent differences in climatic setting; those sites with the greatest proportion of the water class are in milder, maritime climates, with higher temperatures and more

precipitation falling as rain. The bedrock class does not show a clear latitudinal pattern and is most abundant in Deception Island (14 percent) and the McMurdo Dry Valleys (13 percent).

We noted a latitudinal pattern in the presence of vegetation, with the largest proportions of vegetation coverage observed on South Georgia and the South Shetland Islands and no coverage on Alexander Island or the McMurdo Dry Valleys. This is consistent with observations made in Arctic regions, where regions closer to the poles have significantly less vegetation coverage ([Walker et al. 2018](#)). Although no vegetation was detected on Alexander Island or in the McMurdo Dry Valleys, small areas of vegetation have previously been described ([Heywood, Fuchs, and Laws 1977](#); [Pannewitz et al. 2003](#)), though they are typically below the resolution of our classification. The most northern site of South Georgia had significantly more vegetation than any other site (7 percent of the proglacial regions are covered by vegetation; [Figure 6](#)), whereas the McMurdo Dry Valleys and Alexander Island have no detectable vegetation coverage. James Ross Island has very little vegetation cover (<1 percent), whereas the South

Shetland Islands show 2 percent coverage on Byers Peninsula and 1 percent on Deception Island.

Potential drivers of variability

The spatial pattern in sedimentary classes is consistent with the expectation that greater runoff should occur in polar regions with higher temperatures (Syvitski 2002). Increased runoff would result in a greater proportion of the surface being covered by the coarse/wet sediment class. However, the Dry Valleys are an exception to this, with 44 percent of the land covered by coarse or wet sediments (Figure 6). This is likely due to the high relief of the region, allowing for greater mass movement and scree formation (Kirkby and Statham 1975; Doran et al. 2002), and consistent solar radiation during the austral summer facilitating glacier melt and, in combination with subglacial drainage, the formation of large rivers such as the Onyx River (Gooseff et al. 2011; Conovitz et al. 1998; Badgeley et al. 2017). We did not identify any coarse sediment on Alexander Island. The reasoning for this is twofold: (1) an apparent lack of major drainage networks and (2) the scree slopes in this region appear to be small and thin. When viewed from Sentinel-2 images, we could identify only small-size scree slopes and very few streams, consistent with observations made by Heywood, Fuchs, and Laws (1977), who noted that many scree slopes were composed of fine sediments.

The spatial patterns in the wet ice, water, and turbid water classes show more water at the sites further to the north and variability between the east and west, likely due to climatic conditions favoring liquid water on the South Shetland Islands and South Georgia. The disproportionately large amount of water and wet ice on Alexander Island and the James Ross Archipelago relates to the high melt in these areas at the time of image acquisition (Banwell et al. 2021). The bedrock class is most abundant on Deception Island and McMurdo Dry Valleys, owing to ongoing volcanism on Deception Island (Smellie et al. 2002; Rosado et al. 2019) and extensive volcanic history of the McMurdo Dry Valleys (Petford and Mirhadizadeh 2017; Smellie and Martin 2021). This class is also associated with volcanic rocks on James Ross Island (Mlčoch, Nývlt, and Mixa 2020; Jennings et al. 2021) and Byers Peninsula (Gao et al. 2018) and metamorphic rock outcrops on Alexander Island (British Antarctic Survey 1981).

Though latitude accounts for some of the variation in vegetation coverage, it is not the only factor. The sparse vegetation coverage on James Ross Island, despite its relatively low latitude, is consistent with field observations and is logical given its semi-arid climate and high wind speeds (Martin and Peel 1978; Davies et al. 2013; Barták et al. 2015; Nývlt et al. 2016; Hrbáček and Uxa

2020; Kňažková, Nývlt, and Hrbáček 2021; Váczi and Barták 2022). The relatively high vegetation coverage of Byers Peninsula and South Georgia is also logical given the milder maritime climates of the South Shetland Islands and South Georgia, compared to the drier continental climate of Alexander Island and the McMurdo Dry Valleys. Deception Island has less vegetation than the neighboring Byers Peninsula, perhaps due to the impact of ongoing volcanic activity on the island and relatively recent eruptions resulting in unfavorable conditions (Collins 1969; Smith 1988, 2005).

The changing landscape

Out of the five sites we investigated for change, four had similar landscape stability with between 64.2 and 68.2 percent of the land cover remaining unchanged during our study period (Figure 8). Alexander Island, however, varies from this trend with a no change proportion of just 50.2 percent. This is primarily due to the exceptional melt of snow and ice in the region at the time of the second image (2019), which led to more sediment being exposed (ITF) and some lakes and supraglacial lakes (ITT; see Table 2) forming in their place. Eighty-four percent of the change on Alexander Island is due to loss of the ice class, associated with snow and ice melt. This dramatic change in land cover coincides with sustained positive-degree temperatures that occurred in 2019 for the contemporary image and also led to exceptional melt on the George VI ice shelf (Banwell et al. 2021).

Alexander Island is also the exception to a general pattern we observe in the loss of ice across Antarctica. In general, there is a latitudinal pattern in the loss of ice across our sites. If we consider the ITT, ITC, and ITF classes, 45 percent of South Georgia's land cover change is associated with ice loss. In contrast, this value was less than 1 percent for the Dry Valleys, a two orders of magnitude difference. This pattern of ice loss occurs in tandem with a southward increase in the proportion of land cover change associated with sedimentary changes (FTC, CTB, or CTF). Some of these differences in sedimentary class may also be accounted for by the stabilizing and moisture-retaining properties of vegetation coverage (Aalto, le Roux, and Luoto 2013; Klaar et al. 2015), which is higher at the more northerly sites (Figure 6). If we specifically consider the FTC class, we see that it is most abundant on Byers Peninsula. This is likely a product of episodic changes in the flow of streams, which would be expected in the South Shetland Islands given their high rates of precipitation (Bañón et al. 2013). Of the three sites where vegetation was identified in the land cover product, the greatest

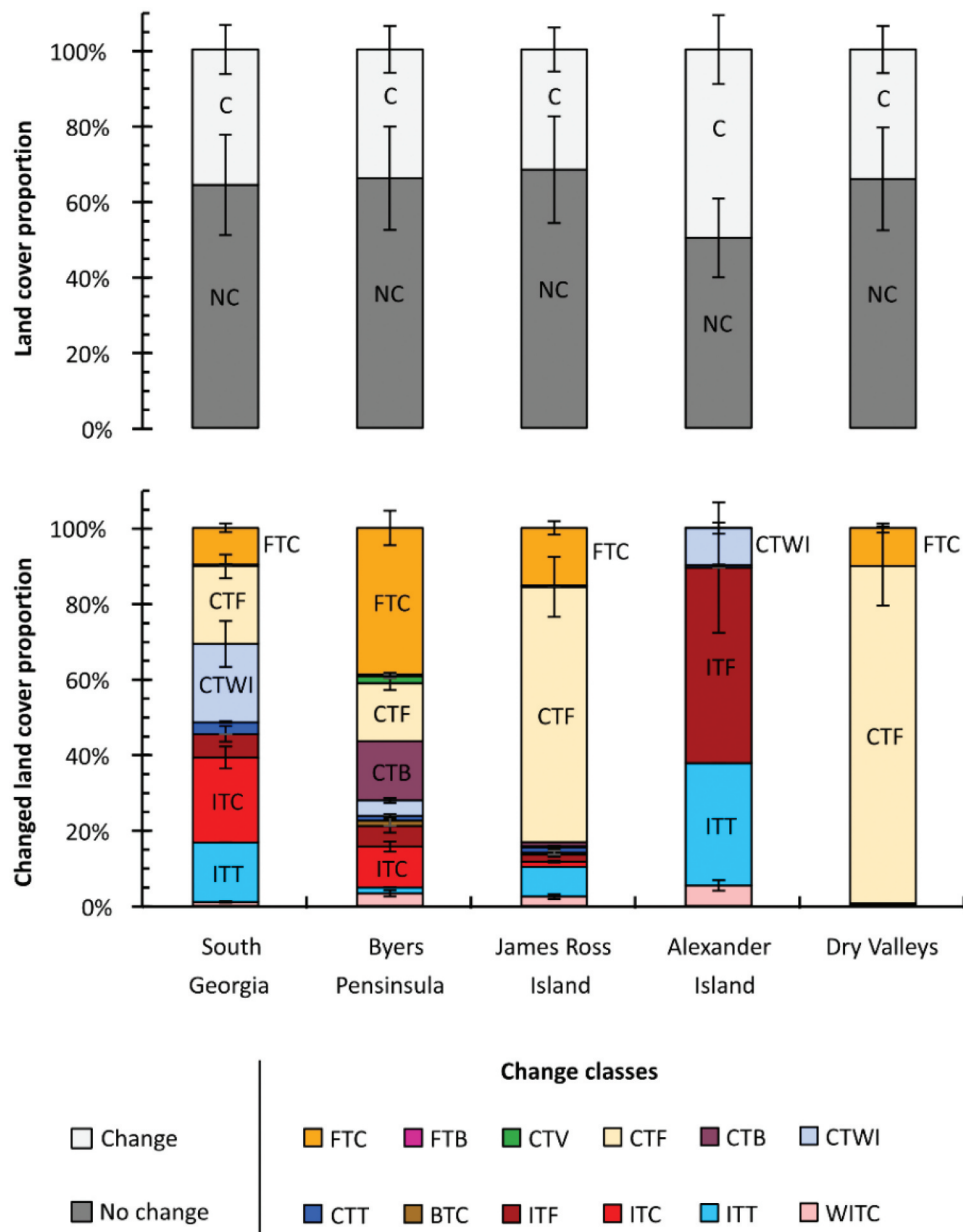


Figure 8. The proportion of the proglacial landscape that has changed at each site analyzed and the makeup of those changed regions.

Table 2. Class-to-class changes and their abbreviations.

Class-to-class change	Abbreviation
Wet ice to coarse/wet sediment	WITC
Ice to fine and dry sediment	ITF
Ice to coarse/wet sediment	ITC
Ice to turbid water	ITT
Coarse/wet sediment to turbid water	CTT
Coarse/wet sediment to wet ice	CTWI
Fine and dry sediment to bedrock	FTB
Coarse/wet sediment to bedrock	CTB
Coarse/wet sediment to fine and dry sediment	CTF
Coarse/wet sediment to vegetation	CTV
Bedrock to coarse/wet sediment	BTC
Fine and dry sediment to coarse/wet sediment	FTC

change was seen on the Byers Peninsula; with 2 percent of its total change accounted for by the CTV class, exceptional vegetation growth in the South Shetland Islands is consistent with previous findings (Torres-Mellado, Jaña, and Casanova-Katny 2011).

Data accuracy

Overall accuracy of land cover product

The overall accuracy of our land cover classification is 95.9 percent. However, this overall value should be taken with caution, because a large proportion of our areas of analysis are covered by ice. This high accuracy represents the fact that our approach is very effective at differentiating ice from land and water. The accuracy of each land class individually provides a more informative assessment of this approach. We find that each proglacial land class has a relatively large standard error, owing to the small number of pixels that we checked (Table 3).

The overall accuracy of the proglacial component of the classification is 77.0 percent, with the greatest percentage uncertainty in the smaller-sized land classes (water and vegetation). Though this overall accuracy is slightly lower than some products (e.g., Malinowski et al. 2020; Pazúr et al. 2022), it should be noted that we achieved this without the availability of extensive training data, making it more comparable with the more moderate accuracies achieved by Chen et al. (2015), for example. The sediment classes typically perform well, with relatively small percentage errors (Table 4). The confusion matrices can be found in the supplementary material (Section 1.5).

Because we were unable to assess the accuracy of the turbid and wet ice classes, we have provided an example

of a classification of each land class, to allow for a qualitative assessment of its accuracy (Figure 7).

When comparing the spectra, we found that our identified classes had distinct spectral signatures that were consistent between locations (Supplementary Section 1.7). Some subtle differences, mostly within the red and near-infrared bands, existed in the sediment and bedrock classes and most likely represent differences in regional geology (M. R. Salvatore et al. 2014). The pattern for vegetation is also notable. Vegetation is typically characterized by peaks in the near-infrared wavelengths; however, we do not observe this in our spectra, likely because the vegetation of Antarctica is dominated by cryptogamic species (e.g., moss), which do not reflect strongly in this band (Váci et al. 2020). The spectra for South Georgia do show a peak in the near-infrared band, consistent with the presence of vascular (leafy) vegetation (Tichit et al. 2024).

We find that our sedimentary classes are similar in spectral pattern (likely due to similarities in geology) but that the coarse/wet class present with lower reflectance values at each site (Supplementary Section 1.7). We interpret this to be due to either its higher water content or its higher grain size (Clark 1999; M. R. Salvatore et al. 2023), which would explain the challenges we found in differentiating between coarse and wet sediments. We note that this distinction is not as clear with the classes on Deception Island. Though we have assigned *K*-means clusters to different classes based on the previously mapped presence of scree and streams, additional caution should be used for interpretations made at this site. The water (water and turbid water) classes are also distinct from each other (Supplementary Section 1.7), primarily on the basis of reflectance values, consistent with previous studies showing that turbid water has higher

Table 3. Accuracy assessment of all land classes.

Class	Error-adjusted area (km ²)	95 Percent confidence (km ²)	Percentage area	Percentage error	n
Water	99.1	45.5	0.2	45.9	9
Ice	44,001.5	219.6	92.2	0.5	2,595
Bedrock	231.3	174.2	0.5	75.3	27
Fine and dry sediment	2,131.5	195.9	4.5	9.2	134
Coarse/wet sediment	1,156.6	174.2	2.4	15.1	114
Vegetation	115.7	56.4	0.2	48.8	10

n < 3,000 because several points landed on cloud-covered parts of the reference images. Percentage error refers to the size of the 95 percent confidence bounds, relative to the error-adjusted area.

Table 4. Accuracy assessment of proglacial classes.

Class	Error-adjusted area (km ²)	95 Percent confidence (km ²)	Percentage area	Percentage error	n
Water	85.7	26.4	2.0	30.9	15
Bedrock	285.5	56.7	6.6	19.9	45
Fine and dry sediment	2,375.5	106.9	54.7	4.5	371
Coarse/wet sediment	1,444.7	108.8	33.3	7.5	257
Vegetation	148.5	40.1	3.4	27.0	34

n < 1,000 because several points landed on cloud-covered parts of the reference images. Percentage error refers to the size of the 95 percent confidence bounds, relative to the error-adjusted area.

reflectance values (Cui et al. 2022). We observed distinctly higher reflectance values for water at Alexander Island, probably because the water at this site is mostly ponded on top of glaciers/ice.

Spatial confidence in land cover product

We produced a map to represent the confidence of our data set (Figure 9), which is notable for its spatial

homogeneity; no individual site appears to be more or less accurate than any other. The McMurdo Dry Valleys have the most “very low confidence” cells, but this is a function of it being the second largest site analyzed, with the largest coverage of proglacial land. Because proglacial classes are less accurate than ice (Tables 3 and 4), it is to be expected that the greatest amount of very low confidence cells would be present here. We also observed

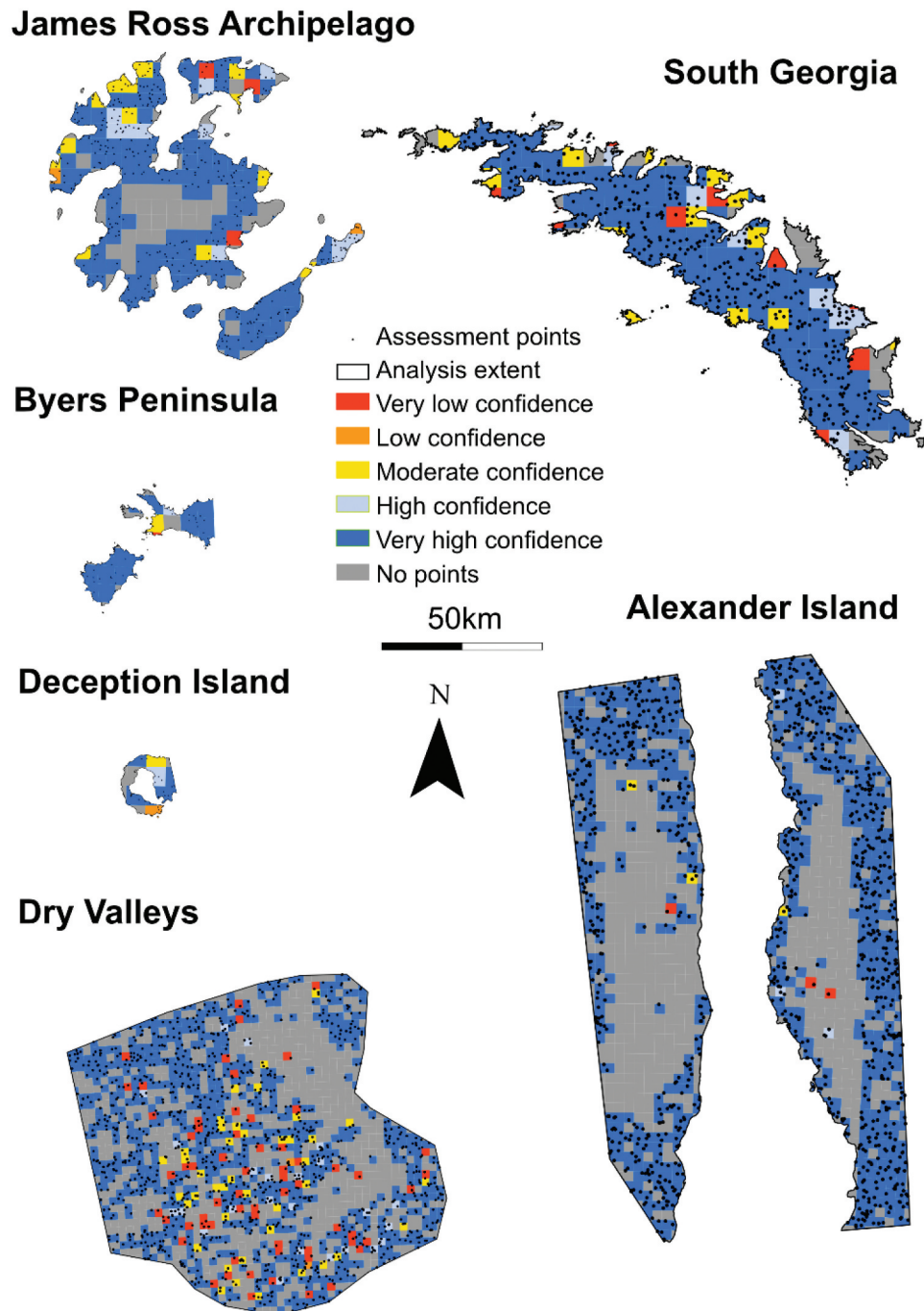


Figure 9. Maps of each site indicating the spatial variability in confidence. Very low confidence = <20 percent of points were accurate; low confidence = 21 to 40 percent; medium confidence = 41 to 60 percent; high confidence = 61 percent to 80 percent; very high confidence = >80 percent.

that many of these very low confidence cells contain only one or two assessment points. This means that just one inaccurate point may result in the cell being classified as very low confidence, when in fact further analysis may reveal that it performs better than represented here.

We also note that the highest accuracy—that is, the regions with the highest density of “very high confidence” cells—is within the ice sheets at each site, which is consistent with the accuracy assessment (Table 3). This is particularly clear on South Georgia and Alexander Island. The regions with “no points” are primarily over the large ice sheets, particularly to the center of James Ross Island, Alexander Island, and the Dry Valleys. Because of the large coverage of ice, many cells were not checked during the accuracy assessment because the random point algorithm does not regularly space points. However, in reality, we are highly confident of cells within the center of ice sheets: they are clearly ice when inspected, and the 92.4 percent accuracy of the ice class (Table 3) suggests that they are very likely to be accurate.

Overall accuracy of change detection

We found that our change detection approach had a total validation accuracy of 80.1 percent. The accuracy varies by class (Table 5), with the most accurate classes being ITT and FTB, albeit from a low sample size. The least accurate class is the coarse/wet sediment to wet ice (CTT) class. However, as stated in section 2.4.1, it is also important to consider the geomorphological processes that the change classes represent. For example, if we merge together classes that represents the same process as CTT (i.e., formation of a lake/formation of a wet area), the error reduces from 60.0 to 5.9 percent.

We can also visually inspect the classes of change by looking at the map of change relative to real changes in

the landscape viewed from satellite images (Figure 10). We can see that our change detection is good at detecting phase changes, such as melting ice (ITF and ITT); in the case of Alexander Island, this highlights the exposure of new sediments, whereas on Snow Island (Byers Peninsula site) this highlights the formation of new proglacial lakes. We are also able to detect more subtle changes in the flow of streams and the presence of wet sediments on James Ross Island (increased river activity, shown by FTC) and Seymour Island (James Ross Archipelago site) with reduced river activity and possible dust deposits.

Data availability

The data used to produce these results, alongside the sampling points for the accuracy assessment and the spatial map of confidence, are available as TIFs and shapefiles from Stringer (2022). The land cover change maps produced from this paper are available from Stringer (2025).

Land class spectra are available in the supplementary materials.

Discussion of study approach and limitations

Methodological approach

Landcover classification

There is a dearth of available data with which to produce an independent training data set necessary for a supervised classification approach (e.g., random forest classification, support vector machine) for a wide-scale land classification in Antarctica (Rodriguez-Galiano et al. 2012). Therefore, we decided to use an unsupervised classification approach. Unsupervised approaches do not require training data sets and instead use the spectral characteristics of each pixel to statistically cluster similar pixels together without user input. The *K*-means

Table 5. Accuracy assessment of land cover change.

Change class	Geomorphological process	Percentage error	Geomorphological process percentage error	n
No change	No change	20.7	20.7	1,563
Wet ice to coarse/wet sediment	Ice melt (land)	25.0	2.8	8
Ice to turbid water	Ice melt (water)	0.0	0.0	13
Ice to coarse/wet sediment	Ice melt (land)	12.7	2.8	79
Ice to fine & dry sediment	Ice melt (land)	33.3	2.8	21
Bedrock to coarse/wet sediment	Sediment deposition	6.7	6.7	15
Coarse/wet sediment to turbid water	Lake formation ^a	60.0	60.0/5.9	10
Coarse/wet sediment to wet ice	Slush–ice formation/lake formation ^a	29.2	29.2/5.9	24
Coarse/wet sediment to bedrock	Erosion	32.3	21.6	127
Coarse/wet sediment to fine & dry sediment	Drying	15.3	15.3	98
Coarse/wet sediment to vegetation	Vegetation formation	30.8	30.8	13
Fine & dry sediment to bedrock	Erosion	0.0	21.6	1
Fine & dry sediment to coarse/wet sediment	Wetting	11.7	11.7	290

Percentage error denotes the proportion of pixels misclassified within that land class. Geomorphological process error denotes the error of the geomorphological process represented by one or more change classes.

^aThere are two possible ways in which classes can be represented as a geomorphological process: either as lake formation and slush-ice formation, or both could be represented as one lake formation class. This affects the resultant geomorphological process error; therefore, two geomorphological process errors are displayed.

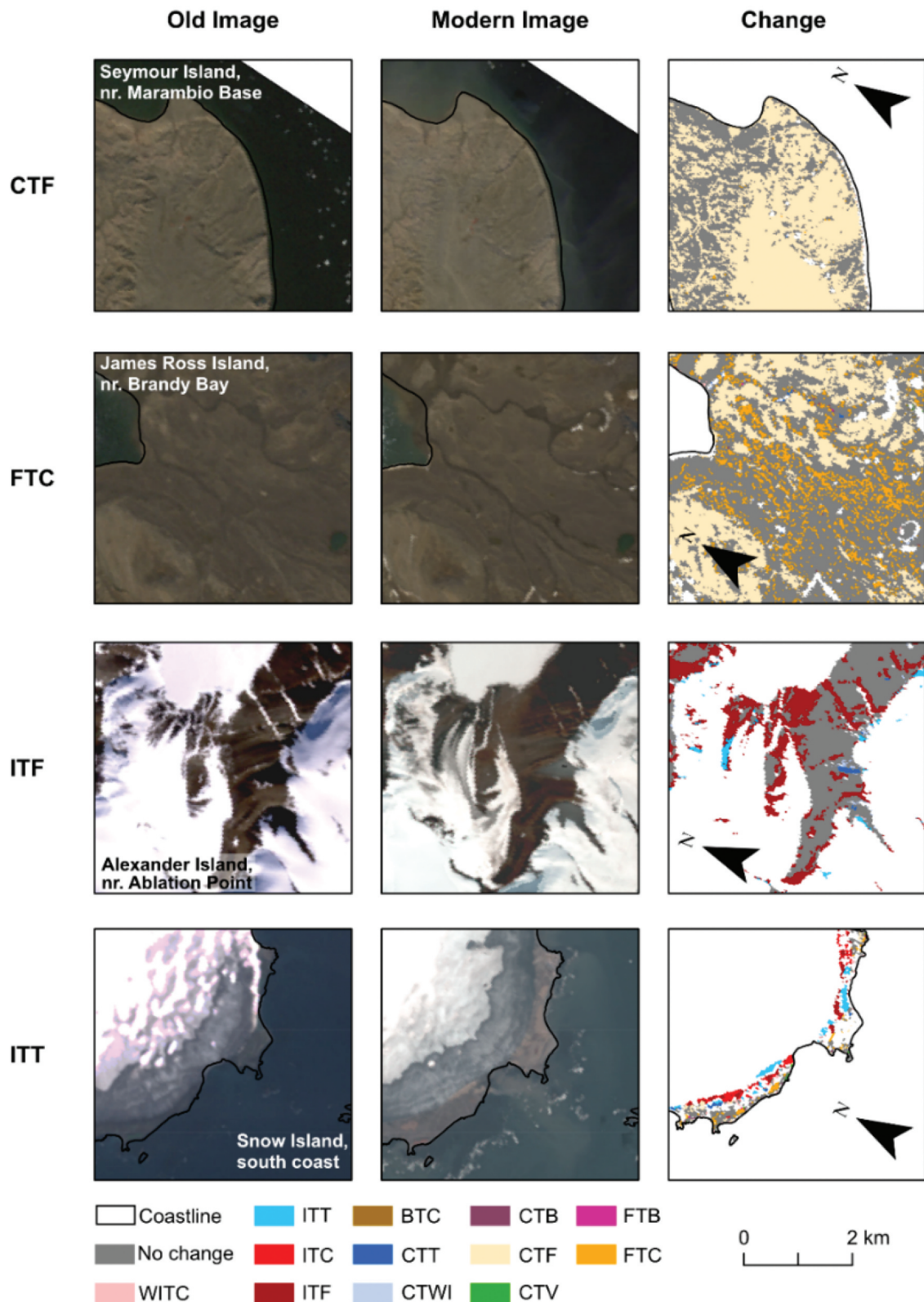


Figure 10. Examples of the four most frequently observed change classes: 86 percent of the change identified in our data can be described by these four classes. The CTF example shows less active river channels in the modern image associated with drier sediments on Seymour Island. FTC shows the opposite, with more active river channels associated with wetter sediments on James Ross Island. The ITF example shows a reduction in the extent of glaciers and snowcover on Alexander Island, and the ITT example shows the development of proglacial lakes following glacier retreat on Snow Island in the South Shetland Islands. Though these four panel sets are designed to highlight the four main change classes, all change classes can be seen within these panels. Modern images are derived from Landsat 8 OLI, and the old images are derived from Landsat 7 ETM+.

algorithm is fully objective and removes the potential to target predefined classes that may be difficult to identify in medium-scale resolution satellite images or that may be in abundance in those areas visited by mapped areas (i.e., those producing training data) but not more widely (Grimes et al. 2024). This approach is particularly useful for large, national/regional-scale spatial analysis and has recently been applied to the classification of Greenland (Mohd Hasmadi, Pakhriazad, and Shahrin 2009; Grimes et al. 2024). Given that land cover data are disparate and incomplete over the study sites, this approach had the added benefit that our field knowledge, as well as information from published maps of relatively small areas (Table 1), could be used to interpret clusters that cover much wider areas.

Change detection

There are several ways in which change detection can be conducted, and these methods have previously been the subject of comprehensive literature reviews (Lu et al. 2004; Tewkesbury et al. 2015). The most commonly used of these techniques is postclassification comparisons of image pairs. This technique involves creating a land cover classification of images in two time periods and then directly comparing the change in classes. Although this method is intuitive, it is flawed because its overall accuracy is reliant on the accuracy of the two land cover products. Individual errors in each land cover map are compounded in the final map of change, resulting in unacceptably high uncertainty values (Lu et al. 2004; Tewkesbury et al. 2015). Change vector analysis determines the changes in the spectral properties of images over time, which allows for a classification that allows the specific type of change to be identified (Bovolo and Bruzzone 2007). Though CVA, as used in this study, has been criticized for being difficult to interpret (Carvalho Júnior et al. 2011), recent advances in this methodology mean that the method has increased the usability of the technique, as well as its ability to identify different types of change (Xu et al. 2018). CVA determines changes in the spectral properties of images over time and has the benefit of avoiding compounding errors (Lu et al. 2004; Tewkesbury et al. 2015).

Study challenges and limitations

Land classification challenges

Previous studies have highlighted three key challenges when it comes to classifying terrestrial landcover: (1)

distinguishing moisture levels in soils/sediments, (2) distinguishing sediment grain size, and (3) the spectral heterogeneity of bedrock. Though we have described land classes that use these terms, because they are useful geomorphological descriptors, we do not argue that we have solved these fundamental challenges associated with distinguishing between these groups spectrally but instead address how our study has arrived at its final classification scheme for these groups.

In terms of moisture, our coarse/wet sediment class came from clustering of mapped features such as scree slopes and braidplains. Previous research has shown that areas of scree slope and moisture sediments are typically associated with lower albedo values (Clark 1999; M. R. Salvatore et al. 2023), which likely accounts for why these groups were clustered together. Nonetheless, combining these two land types in a single class provides a useful indicator of geomorphologically active regions of the landscape.

In our study we found two challenges in classifying bedrock. The first of these challenges was associated with how bedrock is typically mapped versus how we have classified it. For example, in the Dry Valleys, bedrock accounts for 13 percent of the area and the performance of the classification is particularly notable for its ability to pick out an exposed basement sill (Petford and Mirhadizadeh 2017) in Wright Valley. In other studies (e.g., Jennings et al. 2021), bedrock classes are often overrepresented (Figure 4) because the study aims to map geomorphology or geology, rather than surface characteristics such as physical weathering and in situ production of block fields. Moreover, field observations show that boulders and other glacial sediments overlie many of the large igneous extrusions. Therefore, our classification gives a sense of mostly thin surface coverage of exposed solid bedrock. Previous work (e.g., M. R. Salvatore et al. 2014) has highlighted the spectral differences in different types of bedrock; indeed, we also found that several distinct clusters formed during our classification process that highlighted distinct igneous and metamorphic outcrops. For simplicity, these clusters were combined into a single “bedrock” class.

Study limitations and future work

Though we made every effort to minimize the differences in the time of year between image pairs and took further steps to ensure that there was evidence of hydrological activity and minimal snow cover, there remains the possibility that some of the changes we detected were due to differences in growing season or hydrological season or unusual weather events. In particular, those

seasonal factors could affect the area of the vegetation and coarse/wet sediment classes. Future studies should seek to ensure that ground conditions are similar when conducting change detection, the first step of which is to ensure that images are from as close to the same part of the hydrological and growing season as possible. Though it is possible to distinguish between glacial ice and snow (e.g., Awasthi and Varade 2021; Li, Wang, and Wu 2022), many previous land classifications of polar regions have not done so (Wang et al. 2020; Grimes et al. 2024). Some recent studies have made use of snow masking algorithms (e.g., Roland et al. 2024); however, this in itself presents a challenge in that it can alter the land area compared during change detection, which introduces further uncertainty. Therefore, we took the decision to follow the tried-and-tested approach of choosing images with limited visible snow cover.

One of the key challenges of any remote sensing study is validation, and this has been the topic of considerable discussion and review (e.g., Olofsson et al. 2013, 2014). A difficulty found in our study was the lack of existing data sets with which to validate our approach. Furthermore, those independent data sets that do exist were already exploited to aid us in the interpretation of *K*-means clusters (Table 1). Therefore, similar to previous research in remote regions (Grimes et al. 2024), we used our interpretations of higher resolution satellite imagery for validation. This may have introduced some biases through the misclassification of validation points, but we contend that this was preferable to introducing biases from validating our approach against data sets that were used in the initial classification process. The challenges in validating this work highlight the need for further mapping of Antarctic regions based on field observations. Alexander Island, in particular, was difficult to classify due to a lack of supporting material to aid our cluster interpretations; the most recent geological map is from 1981 (British Antarctic Survey 1981), and only limited geomorphological maps of the region exist (M. C. Salvatore 2001). This site highlights the need to collect more high-quality ground data in Antarctica to improve our wider understanding of proglacial environments in the southernmost continent. Even projects to produce high-quality maps in small areas of these remote regions would improve the performance of remote techniques, such as those described in this study.

Summary and conclusions

In this study, we have created a land cover map of the major proglacial regions of sub-Antarctic islands, the

Antarctic Peninsula Region, and the McMurdo Dry Valleys. Given the lack of consistent land cover or geomorphology maps in Antarctica, we used an unsupervised *K*-means clustering approach to classify 30-m-resolution Landsat 8 OLI images by interpreting clusters in a hierarchical approach using our expert judgment and field experience in Antarctica. We present information on the coverage of nine land cover classes: turbid water, water, wet ice, ice, land (nondifferentiated), bedrock, fine sediment, coarse sediment, and vegetation. We mapped eight distinct land surface (plus a no data and land [undifferentiated] class) at 30 m, with an accuracy of 77.0 percent for proglacial classes and 92.2 percent for ice. We also highlighted the spatial pattern in land classes, notably in vegetation and coarse/wet sediment, which are typically more abundant in sites that are more northerly.

Additionally, we analyzed land cover changes in the proglacial regions of Antarctica, which we achieved using a CVA approach at an accuracy of 80.1 percent. Through our analysis of change, we highlighted a latitudinal pattern in ice loss; the proportion of landscape change on South Georgia due to the loss of ice is two orders of magnitude greater than that in the Dry Valleys. This change also occurs in tandem with the opposite pattern occurring in the sediment class changes; this is possibly also influenced by an increase in vegetation coverage in more northern sites. We also highlighted the extensive change in the landscape that has occurred on Alexander Island, where 50 percent of the proglacial coverage has changed this century, likely as a consequence of recent dramatic warming events around the George VI ice shelf.

This data set provides a first step in understanding the makeup of Antarctica's important proglacial regions. It also highlights the need for greater ground-verified data to improve the accuracy of future Antarctic land classifications. We expect that these data will further research in several disciplines, particularly those that focus on ecology, environmental sciences, and atmospheric sciences, and will provide an important first data set for monitoring environmental and ecological change in Antarctica.

Acknowledgments

We thank the Czech Antarctic Research Programme (CARP) for their support of this project, particularly for accommodating C.S. at the Johann Gregor Mendel Research Station on James Ross Island during the austral summer of 2021/22 and at the Nelson Island, South Shetlands, facility during the austral summer of 2022/23. We also thank all of the staff at CARP for their logistical support. Michael Grimes, Elizabeth Mroz, and Eszter Kovacs of the University of Leeds and Jan

Kavan of Masaryk University are thanked for their technical support. The British Antarctic Survey (BAS) and Stephen Jennings provided maps of Alexander Island and James Ross Island, respectively, that made this study possible. BAS also provided other resources, including aerial imagery.

Disclosure statement

No potential conflict of interest was reported by the authors.

Funding

This work is supported by the Leeds-York-Hull Natural Environment Research Council (NERC) Doctoral Training Partnership (DTP) Panorama under Grant NE/S007458/1. The Ministry of Education, Youth and Sports of the Czech Republic project VAN 1/2022 and the Czech Antarctic Foundation funded fieldwork that contributed to part of this work.

ORCID

Christopher D. Stringer  <http://orcid.org/0000-0002-2902-9435>

Jonathan L. Carrivick  <http://orcid.org/0000-0002-9286-5348>

Duncan J. Quincey  <http://orcid.org/0000-0002-7602-7926>

Daniel Nývlt  <http://orcid.org/0000-0002-6876-490X>

Alexis Comber  <http://orcid.org/0000-0002-3652-7846>

Author contributions

C.S. produced the data, conducted the analysis, and wrote the article. A.C. supported the change detection analysis. J.C. conceived the project and supported C.S. in writing the first draft of the article. D.Q. and D.N. reviewed the article prior to submission. All authors contributed to the writing of the article.

Code availability

Stringer, C.D. (2022). Contemporary (2016–2020) land cover across West Antarctica and the McMurdo Dry Valleys [Code] (Version 1). Zenodo. <https://doi.org/10.5281/zenodo.6720051>

Stringer, C.D. (2023). 21st century land cover change across the major proglacial regions of West Antarctica and the McMurdo Dry Valleys [Code]. (Version v1). Zenodo. <https://doi.org/10.5281/zenodo.7991208>

References

- Aalto, J., P.C. le Roux, and M. Luoto. 2013. Vegetation mediates soil temperature and moisture in arctic-alpine environments. *Arctic, Antarctic, and Alpine Research* 45, no. 4: 429–39. doi:10.1657/1938-4246-45.4.429.
- Adelabu, S., O. Mutanga, and E. Adam. 2015. Testing the reliability and stability of the internal accuracy assessment of random forest for classifying tree defoliation levels using different validation methods. *Geocarto International* 30, no. 7: 810–21. doi:10.1080/10106049.2014.997303.
- Awasthi, S., and D. Varade. 2021. Recent advances in the remote sensing of alpine snow: A review. *GIScience & Remote Sensing* 58, no. 6: 852–88. doi:10.1080/15481603.2021.1946938.
- Badgeley, J.A., E.C. Pettit, C.G. Carr, S. Tulaczyk, J. A. Mikucki, and W.B. Lyons. 2017. An englacial hydrologic system of brine within a cold glacier: Blood Falls, McMurdo Dry Valleys, Antarctica. *Journal of Glaciology* 63, no. 239: 387–400. doi:10.1017/jog.2017.16.
- Ballantyne, C.K. 2008. After the Ice: Holocene geomorphic activity in the Scottish Highlands. *Scottish Geographical Journal* 124, no. 1: 8–52. doi:10.1080/14702540802300167.
- Ban, Y., P. Gong, and C. Giri. 2015. Global land cover mapping using Earth observation satellite data: Recent progresses and challenges. *ISPRS Journal of Photogrammetry and Remote Sensing* 103: 1–6. doi:10.1016/j.isprsjprs.2015.01.001.
- Bannister, D., and J. King. 2015. Föhn winds on South Georgia and their impact on regional climate. *Weather* 70, no. 11: 324–9. doi:10.1002/wea.2548.
- Bañón, M., A. Justel, D. Velázquez, and A. Quesada. 2013. Regional weather survey on Byers Peninsula, Livingston Island, South Shetland Islands, Antarctica. *Antarctic Science* 25, no. 2: 146–56. doi:10.1017/S0954102012001046.
- Banwell, A.F., R. Tri Datta, R.L. Dell, M. Moussavi, L. Brucker, G. Picard, C.A. Shuman, and L.A. Stevens. 2021. The 32-year record-high surface melt in 2019/2020 on the northern George VI Ice Shelf, Antarctic Peninsula. *The Cryosphere* 15, no. 2: 909–25. doi:10.5194/tc-15-909-2021.
- Barták, M., P. Váczi, Z. Stachoň, and S. Kubešová. 2015. Vegetation mapping of moss-dominated areas of northern part of James Ross Island (Antarctica) and a suggestion of protective measures. *Czech Polar Reports* 5, no. 1: 75–87. doi:10.5817/CPR2015-1-8.
- Bojinski, S., M. Verstraete, T.C. Peterson, C. Richter, A. Simmons, and M. Zemp. 2014. The concept of essential climate variables in support of climate research, applications, and policy. *Bulletin of the American Meteorological Society* 95, no. 9: 1431–43. doi:10.1175/BAMS-D-13-00047.1.
- Bovolo, F., and L. Bruzzone. 2007. A theoretical framework for unsupervised change detection based on change vector analysis in the polar domain. *IEEE Transactions on Geoscience and Remote Sensing* 45, no. 1: 218–36. doi:10.1109/TGRS.2006.885408.
- British Antarctic Survey. 1981. *British Antarctic Territory geological map. Sheet 4. Alexander Island* 1:500000. Cambridge: British Antarctic Survey. <https://www.bas.ac.uk/data/our-data/maps>.
- Brown, C.F., S.P. Brumby, B. Guzder-Williams, T. Birch, S. B. Hyde, J. Mazzariello, W. Czerwinski, et al. 2022. Dynamic world, near real-time global 10 m land use land cover mapping. *Scientific Data* 9, no. 1: 251. doi:10.1038/s41597-022-01307-4.
- Brussaard, C.P.D., S.W. Wilhelm, F. Thingstad, M. G. Weinbauer, G. Bratbak, M. Heldal, S.A. Kimmance, et al. 2008. Global-scale processes with a nanoscale drive: The role of marine viruses. *The ISME Journal* 2, no. 6: 575–8. doi:10.1038/ismej.2008.31.

- Burton-Johnson, A., M. Black, P.T. Fretwell, and J. Kaluza-Gilbert. 2016. An automated methodology for differentiating rock from snow, clouds and sea in Antarctica from Landsat 8 imagery: A new rock outcrop map and area estimation for the entire Antarctic continent. *The Cryosphere* 10, no. 4: 1665–77. doi:10.5194/tc-10-1665-2016.
- Carrasco, J.F., D. Bozkurt, and R.R. Cordero. 2021. A review of the observed air temperature in the Antarctic Peninsula. Did the warming trend come back after the early 21st hiatus? *Polar Science* 28: 100653. doi:10.1016/j.polar.2021.100653.
- Carrivick, J.L., T. Heckmann, M. Fischer, and B. Davies. 2019. *An inventory of proglacial systems in Austria, Switzerland and across Patagonia*. Cham: Springer International Publishing.
- Carrivick, J.L., T. Heckmann, A. Turner, and M. Fischer. 2018. An assessment of landform composition and functioning with the first proglacial systems dataset of the central European Alps. *Geomorphology* 321: 117–28. doi:10.1016/j.geomorph.2018.08.030.
- Carvalho Júnior, O.A., R.F. Guimarães, A.R. Gillespie, N. C. Silva, and R.A.T. Gomes. 2011. A new approach to change vector analysis using distance and similarity measures. *Remote Sensing* 3, no. 11: 2473–93. doi:10.3390/rs3112473.
- Chasmer, L., C. Mahoney, K. Millard, K. Nelson, D. Peters, M. Merchant, C. Hopkinson, et al. 2020. Remote sensing of Boreal Wetlands 2: Methods for evaluating boreal wetland ecosystem state and drivers of change. *Remote Sensing* 12, no. 8: 1321. doi:10.3390/rs12081321.
- Chen, J., A. Liao, X. Cao, L. Chen, and X. Chen, X., C. He, G. Han, S. Peng, et al. 2015. Global land cover mapping at 30m resolution: A POK-based operational approach. *ISPRS Journal of Photogrammetry & Remote Sensing* 103: 7–27. doi:10.1016/j.isprsjprs.2014.09.002.
- Chen, W., X. Li, and L. Wang. 2019. Fine land cover classification in an open pit mining area using optimized support vector machine and WorldView-3 imagery. *Remote Sensing* 12, no. 1: 82. doi:10.3390/rs12010082.
- Chinn, T., and P. Mason. 2016. The first 25 years of the hydrology of the Onyx River, Wright Valley, Dry Valleys, Antarctica. *Polar Record* 52, no. 1: 16–65. doi:10.1017/S0032247415000212.
- Clapperton, C.M. 1971. *Geomorphology of the stromness bay-Cumberland bay area, South Georgia*. London: British Antarctic Survey.
- Clark, R. N. 1999. Spectroscopy of rocks and minerals, and principles of spectroscopy. In vol. 3, *Manual of Remote Sensing, Remote Sensing for the Earth Sciences*, ed. A. N. Rencz, 3–58. New York: John Wiley and Sons.
- Collins, N.J. 1969. The effects of volcanic activity on the vegetation of Deception Island. *British Antarctic Survey Bulletin* 21: 79–94.
- Conovitz, P.A., D.M. Mcknight, L.H. Macdonald, A. G. Fountain, and H.R. House. 1998. Hydrologic processes influencing streamflow variation in Fryxell Basin, Antarctica. In *Ecosystem dynamics in a polar desert: The McMurdo Dry Valleys, Antarctica*, ed. J.C. Priscu, 93–108. Washington, DC: American Geophysical Union. doi:10.1029/AR072p0093.
- Convey, P., and R.I.L. Smith. 2007. Responses of terrestrial Antarctic ecosystems to climate change. In *Plants and climate change*, ed. J. Rozema, R. Aerts, and H. Cornelissen, 1–12. Dordrecht: Springer. Netherlands.
- Costa, A., P. Molnar, L. Stutenbecker, M. Bakker, T.A. Silva, F. Schlunegger, S.N. Lane, J.L. Loizeau, and S. Girardclos. 2018. Temperature signal in suspended sediment export from an Alpine catchment. *Hydrology and Earth System Sciences* 22, no. 1: 509–28. doi:10.5194/hess-22-509-2018.
- Cox, S.C., B. Smith Lyttle, S. Elkind, C. Smith Siddoway, P. Morin, G. Capponi, T. Abu-Alam, et al. 2023. A continent-wide detailed geological map dataset of Antarctica. *Scientific Data* 10, no. 1. doi:10.1038/s41597-023-02152-9.
- Cui, M., Y. Sun, C. Huang, and M. Li. 2022. Water turbidity retrieval based on UAV hyperspectral remote sensing. *Water* 14, no. 1: 128. doi:10.3390/w14010128.
- da Rosa, K.K., C. Perondi, B.K. Veetil, J.D. Auger, and J. C. Simões. 2020. Contrasting responses of land-terminating glaciers to recent climate variations in King George Island, Antarctica. *Antarctic Science* 32, no. 5: 398–407. doi:10.1017/S0954102020000279.
- Davies, B.J., J.L. Carrivick, N.F. Glasser, M.J. Hambrey, and J. L. Smellie. 2012. Variable glacier response to atmospheric warming, northern Antarctic Peninsula, 1988–2009. *Cryosphere* 6, no. 5: 1031–48. doi:10.5194/tc-6-1031-2012.
- Davies, B.J., N.F. Glasser, J.L. Carrivick, M.J. Hambrey, J. L. Smellie, and D. Nývlt. 2013. Landscape evolution and ice-sheet behaviour in a semi-arid polar environment: James Ross Island, NE Antarctic Peninsula. *Geological Society, London, Special Publications* 381, no. 1: 353–95. doi:10.1144/SP381.1.
- Davies, B.J., M.J. Hambrey, N.F. Glasser, T. Holt, A. Rodés, J. L. Smellie, J.L. Carrivick, and S.P.E. Blockley. 2017. Ice-dammed lateral lake and epishelf lake insights into Holocene dynamics of Marguerite Trough Ice Stream and George VI Ice Shelf, Alexander Island, Antarctic Peninsula. *Quaternary Science Reviews* 177: 189–219. doi:10.1016/j.quascirev.2017.10.016.
- Doran, P.T., C.P. McKay, G.D. Clow, G.L. Dana, A. G. Fountain, T. Nylen, and W.B. Lyons. 2002. Valley floor climate observations from the McMurdo dry valleys, Antarctica, 1986–2000. *Journal of Geophysical Research: Atmospheres* 107, no. 24: 4772. doi:10.1029/2001JD002045.
- Doran, P.T., R.A. Wharton, and W.B. Lyons. 1994. Paleolimnology of the McMurdo dry valleys, Antarctica. *Journal of Paleolimnology* 10, no. 2: 85–114. doi:10.1007/BF00682507.
- Engel, Z., K. Láská, J. Kavan, and J. Smolíková. 2023. Persistent mass loss of Triangular Glacier, James Ross Island, north-eastern Antarctic Peninsula. *Journal of Glaciology* 69, no. 273: 27–39. doi:10.1017/jog.2022.42.
- Engel, Z., K. Láská, D. Nývlt, and Z. Stachoň. 2018. Surface mass balance of small glaciers on James Ross Island, north-eastern Antarctic Peninsula, during 2009–2015. *Journal of Glaciology* 64, no. 245: 349–61. doi:10.1017/jog.2018.17.
- Farr, T.G., P.A. Rosen, E. Caro, R. Crippen, R. Duren, S. Hensley, M. Kobrick, et al. 2007. The shuttle radar topography mission. *Reviews of Geophysics* 45, no. 2: RG2004. doi:10.1029/2005RG000183.

- Friedl, M.A., D. Sulla-Menashe, B. Tan, A. Schneider, N. Ramankutty, A. Sibley, and X. Huang. 2010. MODIS Collection 5 global land cover: Algorithm refinements and characterization of new datasets. *Remote Sensing of Environment* 114, no. 1: 168–82. doi:10.1016/j.rse.2009.08.016.
- Frohn, R.C., M. Reif, C. Lane, and B. Autrey. 2009. Satellite remote sensing of isolated wetlands using object-oriented classification of Landsat-7 data. *Wetlands* 29, no. 3: 931–41. doi:10.1672/08-194.1.
- Galera, H., A. Znój, K.J. Chwedorzewska, and M. Wódkiewicz. 2021. Evaluation of factors influencing the eradication of annual bluegrass (*Poa annua* L.) from Point Thomas Oasis, King George Island, Maritime Antarctica. *Polar Biology* 44, no. 12: 2255–68. doi:10.1007/s00300-021-02941-1.
- Gao, L., Y. Zhao, Z. Yang, J. Liu, X. Liu, S.H. Zhang, and J. Pei. 2018. New paleomagnetic and ⁴⁰Ar/³⁹Ar geochronological results for the South Shetland Islands, West Antarctica, and their tectonic implications. *Journal of Geophysical Research: Solid Earth* 123, no. 1: 4–30. doi:10.1002/2017JB014677.
- GCOS. 2010. *Implementation plan for the global observing system for climate in support of the UNFCCC (2010 update)*, 186. Geneva: World Meteorological society.
- Gerrish, L., P. Fretwell, and P. Cooper. 2020. *High resolution vector polygons of Antarctic rock outcrop (7.3) [Data set]*. Cambridge, UK: UK Polar Data Centre, Natural Environment Research Council. UK Research & Innovation.
- Gerrish, L., P. Fretwell, and P. Cooper. 2021. *Medium resolution vector polygons of the Antarctic coastline (Version 7.4) [Data set]*. Cambridge, UK: UK Polar Data Centre, Natural Environment Research Council, UK Research & Innovation.
- Gong, P., X. Li, J. Wang, Y. Bai, B. Chen, T. Hu, X. Liu, et al. 2020. Annual maps of global artificial impervious area (GAIA) between 1985 and 2018. *Remote Sensing of Environment* 236: 111510. doi:10.1016/j.rse.2019.111510.
- Gooseff, M.N., D.M. McKnight, P. Doran, A.G. Fountain, and W.B. Lyons. 2011. Hydrological connectivity of the landscape of the McMurdo Dry Valleys, Antarctica. *Geography Compass* 5, no. 9: 666–81. doi:10.1111/j.1749-8198.2011.00445.x.
- Grimes, M., J.L. Carrivick, M.W. Smith, and A.J. Comber. 2024. Land cover changes across Greenland dominated by a doubling of vegetation in three decades. *Scientific Reports* 14, no. 1: 3120. doi:10.1038/s41598-024-52124-1.
- Harangozo, S.A., S.R. Colwell, and J.C. King. 1997. An analysis of a 34-year air temperature record from Fossil Bluff (71°S, 68°W), Antarctica. *Antarctic Science* 9, no. 3: 355–63. doi:10.1017/S0954102097000436.
- Heywood, R.B., V.E. Fuchs, and R.M. Laws. 1977. A limnological survey of the Ablation Point area, Alexander Island, Antarctica. *Philosophical Transactions of the Royal Society of London B: Biological Sciences* 279, no. 963: 39–54. doi:10.1098/rstb.1977.0070.
- Howat, I.M., C. Porter, B.E. Smith, M.-J. Noh, and P. Morin. 2019. The reference elevation model of Antarctica. *The Cryosphere* 13, no. 2: 665–74. doi:10.5194/tc-13-665-2019.
- Hrbáček, F., and T. Uxa. 2020. The evolution of a near-surface ground thermal regime and modeled active-layer thickness on James Ross Island, Eastern Antarctic Peninsula, in 2006–2016. *Permafrost and Periglacial Processes* 31, no. 1: 141–55. doi:10.1002/ppp.2018.
- Hughes, K.A., O.L. Pescott, J. Peyton, T. Adriaens, E.J. Cottier-Cook, G. Key, W. Rabitsch, et al. 2020. Invasive non-native species likely to threaten biodiversity and ecosystems in the Antarctic Peninsula region. *Global Change Biology* 26, no. 4: 2702–16. doi:10.1016/j.jembe.2019.151227.
- Humlum, O., A. Instanes, and J.L. Sollid. 2003. Permafrost in Svalbard: A review of research history, climatic background and engineering challenges. *Polar Research* 22, no. 2: 191–215. doi:10.1111/j.1751-8369.2003.tb00107.x.
- Jennings, S.J.A., B.J. Davies, D. Nývlt, N.F. Glasser, Z. Engel, F. Hrbáček, J.L. Carrivick, B. Mlčoch, and M.J. Hambrey. 2021. Geomorphology of Ulu Peninsula, James Ross Island, Antarctica. *Journal of Maps* 17, no. 2: 125–39. doi:10.1080/17445647.2021.1893232.
- Kaplan Pastíriková, L., F. Hrbáček, T. Uxa, and K. Láška. 2023. Permafrost table temperature and active layer thickness variability on James Ross Island, Antarctic Peninsula, in 2004–2021. *Science of the Total Environment* 869: 161690. doi:10.1016/j.scitotenv.2023.161690.
- Kavan, J. 2021. Fluvial transport in the deglaciated Antarctic catchment–Bohemian Stream, James Ross Island. *Geografiska Annaler, Series A: Physical Geography* 104, no. 1: 1–10. doi:10.1080/04353676.2021.2010401.
- Kavan, J., J. Ondruch, D. Nývlt, F. Hrbáček, J.L. Carrivick, and K. Láška. 2017. Seasonal hydrological and suspended sediment transport dynamics in proglacial streams, James Ross Island, Antarctica. *Geografiska Annaler: Series A, Physical Geography* 99, no. 1: 38–55. doi:10.1080/04353676.2016.1257914.
- Kirkby, M.J., and I. Statham. 1975. Surface stone movement and scree formation. *The Journal of Geology* 83, no. 3: 349–62.
- Klaar, M.J., C. Kidd, E. Malone, R. Bartlett, G. Pinay, F. S. Chapin, and A. Milner. 2015. Vegetation succession in deglaciated landscapes: Implications for sediment and landscape stability. *Earth Surface Processes and Landforms* 40, no. 8: 1088–100. doi:10.1002/esp.3691.
- Kňázková, M., D. Nývlt, and F. Hrbáček. 2021. Slope processes connected with snow patches in semi-arid ice-free areas of James Ross Island, Antarctic Peninsula. *Geomorphology* 373: 107479. doi:10.1016/j.geomorph.2020.107479.
- Lea, J.M. 2018. The Google Earth engine digitisation tool (GEEDiT) and the margin change quantification tool (MaQiT) – Simple tools for the rapid mapping and quantification of changing Earth surface margins. *Earth Surface Dynamics* 6, no. 3: 551–61. doi:10.5194/esurf-6-551-2018.
- Lee, J.R., B. Raymond, T.J. Bracegirdle, I. Chadès, R.A. Fuller, J.D. Shaw, and A. Terauds. 2017. Climate change drives expansion of Antarctic ice-free habitat. *Nature* 547, no. 7661: 49–54. doi:10.1038/nature22996.
- Łepkowska, E., and Ł. Stachnik. 2018. Which Drivers Control the Suspended Sediment Flux in a High Arctic Glacierized Basin (Werenskioldbreen, Spitsbergen)? *Water* 10, no. 10: 1408. doi:10.3390/w10101408.
- Li, X., N. Wang, and Y. Wu. 2022. Automated glacier snow line altitude calculation method using landsat series images in the Google Earth engine platform. *Remote Sensing* 14, no. 10: 2377. doi:10.3390/rs14102377.
- Lopez-Martinez, J., M. R. A. Thomson, A. Arche, S. Bjorck, J. C. Ellis-Evans, B. Hathway, Hernandez-Cifuentes, et al. 1996. *Geomorphological map of Byers Peninsula, Livingston*

- Island 1:25 000. GEOMAP Series, Sheet 5-A. Cambridge: British Antarctic Survey.
- Lu, D., P. Mausel, E. Brondizio, and E. Moran. 2004. Change detection techniques. *International Journal of Remote Sensing* 25, no. 12: 2365–401. doi:10.1080/0143116031000139863.
- Maat, D.S., R.J.W. Visser, and C.P.D. Brussaard. 2019. Virus removal by glacier-derived suspended fine sediment in the Arctic. *Journal of Experimental Marine Biology and Ecology* 521: 151227. doi:10.1016/j.jembe.2019.151227.
- Malinowski, R., S. Lewiński, M. Rybicki, E. Gromny, M. Jenerowicz, M. Krupiński, A. Nowakowski, et al. 2020. Automated production of a land cover/use map of Europe based on Sentinel-2 imagery. *Remote Sensing* 12, no. 21: 3523. doi:10.3390/rs12213523.
- Marchant, D.R., and J.W. Head. 2007. Antarctic dry valleys: Microclimate zonation, variable geomorphic processes, and implications for assessing climate change on Mars. *Icarus* 192, no. 1: 187–222. doi:10.1016/j.icarus.2007.06.018.
- Martin, P.J., and D.A. Peel. 1978. the spatial distribution of 10 m temperatures in the Antarctic Peninsula. *Journal of Glaciology* 20, no. 83: 311–7. doi:10.3189/S0022143000013861.
- Mink, S., J. López-Martínez, A. Maestro, J. Garrote, J. A. Ortega, E. Serrano, J.J. Durán, and T. Schmid. 2014. Insights into deglaciation of the largest ice-free area in the South Shetland Islands (Antarctica) from quantitative analysis of the drainage system. *Geomorphology* 225: 4–24. doi:10.1016/j.geomorph.2014.03.028.
- Mlčoch, B., D. Nývlt, and P. Mixa. 2020. *Geological map of James Ross Island–Northern part 1: 25,000*. <https://cgs.gov.cz/en/about-us/current-events/publication-of-the-first-geological-map-of-the-northern-part-of-james-ross>.
- Mohd Hasmadi, I., H.Z. Pakhriazad, and M.F. Shahrin. 2009. Evaluating supervised and unsupervised techniques for land cover mapping using remote sensing data. *Malaysian Journal of Society and Space* 5, no. 1: 1–10.
- Molina-Montenegro, M.A., F. Carrasco-Urra, C. Rodrigo, P. Convey, F. Valladares, and E. Gianoli. 2012. Occurrence of the non-native annual bluegrass on the Antarctic mainland and its negative effects on native plants. *Conservation Biology* 26, no. 4: 717–23. doi:10.1111/j.1523-1739.2012.01865.x.
- Mulvaney, R., N.J. Abram, R.C.A. Hindmarsh, C. Arrowsmith, L. Fleet, J. Triest, L.C. Sime, O. Alemany, and S. Foord. 2012. Recent Antarctic Peninsula warming relative to Holocene climate and ice-shelf history. *Nature* 489, no. 7414: 141–4. doi:10.1038/nature11391.
- Nedbalová, L., D. Nývlt, J. Kopáček, M. Šobr, and J. Elster. 2013. Freshwater lakes of Ulu Peninsula, James Ross Island, north-east Antarctic Peninsula: Origin, geomorphology and physical and chemical limnology. *Antarctic Science* 25, no. 3: 358–72. doi:10.1017/S0954102012000934.
- Nývlt, D., M.N. Fišáková, M. Barták, Z. Stachoň, V. Pavel, B. Mlčoch, and K. Láška. 2016. Death age, seasonality, taphonomy and colonization of seal carcasses from Ulu Peninsula, James Ross Island, Antarctic Peninsula. *Antarctic Science* 28, no. 1: 3–16. doi:10.1017/S095410201500036X.
- Oliva, M., D. Antoniades, S. Giral, I. Granados, S. Pla-Rabes, M. Toro, E.J. Liu, J. Sanjurjo, and G. Vieira. 2016. The Holocene deglaciation of the Byers Peninsula (Livingston Island, Antarctica) based on the dating of lake sedimentary records. *Geomorphology* 261: 89–102. doi:10.1016/j.geomorph.2016.02.029.
- Oliva, M., F. Navarro, F. Hrbáček, A. Hernández, D. Nývlt, P. Pereira, J. Ruiz-Fernández, and R. Trigo. 2017. Recent regional climate cooling on the Antarctic Peninsula and associated impacts on the cryosphere. *Science of the Total Environment* 580: 210–23. doi:10.1016/j.scitotenv.2016.12.030.
- Olofsson, P., G.M. Foody, M. Herold, S.V. Stehman, C. E. Woodcock, and M.A. Wulder. 2014. Good practices for estimating area and assessing accuracy of land change. *Remote Sensing of Environment* 148: 42–57. doi:10.1016/j.rse.2014.02.015.
- Olofsson, P., G.M. Foody, S.V. Stehman, and C.E. Woodcock. 2013. Making better use of accuracy data in land change studies: Estimating accuracy and area and quantifying uncertainty using stratified estimation. *Remote Sensing of Environment* 129: 122–31. doi:10.1016/j.rse.2012.10.031.
- Pannewitz, S., T.G.A. Green, C. Scheidegger, M. Schlensog, and B. Schroeter. 2003. Activity pattern of the moss *Hennediella heimii* (Hedw.) Zand in the Dry Valleys, Southern Victoria Land, Antarctica during the mid-austral summer. *Polar Biology* 26, no. 8: 545–51. doi:10.1007/s00300-003-0518-8.
- Pazúr, R., N. Huber, D. Weber, C. Ginzler, and B. Price. 2022. A national extent map of cropland and grassland for Switzerland based on Sentinel-2 data. *Earth System Science Data* 14, no. 1: 295–305. doi:10.5194/essd-14-295-2022.
- Petford, N., and S. Mirhadizadeh. 2017. Image-based modelling of lateral magma flow: The Basement Sill, Antarctica. *Royal Society Open Science* 4, no. 5: 161083. doi:10.1098/rsos.161083.
- Phiri, D., and J. Morgenroth. 2017. Developments in Landsat land cover classification methods: A review. *Remote Sensing* 9, no. 9: 967. doi:10.3390/rs9090967.
- Raup, B., A. Racoviteanu, S.J.S. Khalsa, C. Helm, R. Armstrong, and Y. Arnaud. 2007. The GLIMS geospatial glacier database: A new tool for studying glacier change. *Global and Planetary Change* 56, no. 1–2: 101–10. doi:10.1016/j.gloplacha.2006.07.018.
- Rodriguez-Galiano, V.F., B. Ghimire, J. Rogan, M. Chica-Olmo, and J.P. Rigol-Sanchez. 2012. An assessment of the effectiveness of a random forest classifier for land-cover classification. *ISPRS Journal of Photogrammetry and Remote Sensing* 67, no. 1: 93–104. doi:10.1016/j.isprsjprs.2011.11.002.
- Roland, T. P., O. T. Bartlett, D. J. Charman, K. Anderson, D. A. Hodgson, M. J. Amesbury, I. Maclean, P. T. Fretwell, and A. Fleming. 2024. Sustained greening of the Antarctic Peninsula observed from satellites. *Nature Geoscience* 17: 1121–6. doi:10.1038/s41561-024-01564-5.
- Roman, M., L. Nedbalová, T.J. Kohler, J.M. Lirio, S.H. Coria, J. Kopáček, P.A. Vignoni, et al. 2019. Lacustrine systems of Clearwater Mesa (James Ross Island, north-eastern Antarctic Peninsula): Geomorphological setting and limnological characterization. *Antarctic Science* 31, no. 4: 169–88. doi:10.1017/S0954102019000178.
- Rosado, B., A. Fernández-Ros, M. Berrocoso, G. Prates, J. Gárate, A. de Gil, and A. Geyer. 2019. Volcano-tectonic dynamics of Deception Island (Antarctica): 27 years of GPS observations (1991–2018). *Journal of Volcanology and*

- Geothermal Research* 381: 57–82. doi:10.1016/j.jvolgeores.2019.05.009.
- Ruiz-Fernández, J., M. Oliva, and C. García-Hernández. 2017. Topographic and geomorphologic controls on the distribution of vegetation formations in Elephant Point (Livingston Island, Maritime Antarctica). *Science of the Total Environment* 587–588: 340–9. doi:10.1016/j.scitotenv.2017.02.158.
- Salvatore, M.C. 2001. Geomorphological sketch map of the Fossil Bluff area (Alexander Island, Antarctica) mapped from aerial photographs. *Antarctic Science* 13, no. 1: 75–8. doi:10.1017/S0954102001000116.
- Salvatore, M.R., J.E. Barrett, L.E. Fackrell, E.R. Sokol, J.S. Levy, L.C. Kuentz, M.N. Gooseff, et al. 2023. The distribution of surface soil moisture over space and time in Eastern Taylor Valley, Antarctica. *Remote Sensing* 15, no. 12: 3170. doi:10.3390/rs15123170.
- Salvatore, M.R., J.F. Mustard, J.W. Head, D.R. Marchant, and M.B. Wyatt. 2014. Characterization of spectral and geochemical variability within the Ferrar Dolerite of the McMurdo Dry Valleys, Antarctica: Weathering, alteration, and magmatic processes. *Antarctic Science* 26, no. 1: 49–68. doi:10.1017/S0954102013000254.
- Secretariat of the Antarctic Treaty. 2022. ASPA 140: Parts of Deception Island. <https://www.ats.aq/devph/en/apa-data-base/45#:~:text=Deception%20Island%20is%20an%20active,feature%20associated%20with%20each%20site>.
- Smellie, J.L. 2013. Geological map of James Ross Island 1. BAS GEOMAP 2 Series, Sheet 5. James Ross Island Volcanic Group. British Antarctic Survey, Cambridge.
- Smellie, J.L., J. Lopez-Martinez Geomorphological, J. Lopez-Martinez, E. Serrano, J. Rey, R.K. Headland, F. Hernandez-Cifuentes, et al. 2002. *Geology and geomorphology of Deception Island*. Cambridge, UK: British Antarctic Survey.
- Smellie, J.L., and A.P. Martin. 2021. Chapter 5.2a Erebus Volcanic Province: Volcanology. *Geological Society, London, Memoirs* 55, no. 1: 415–46. doi:10.1144/M55-2018-62.
- Smith, R.I.L. 1988. Botanical survey of Deception Island. *British Antarctic Survey Bulletin* 80: 129–36.
- Smith, R.I.L. 2005. The thermophilic bryoflora of Deception Island: Unique plant communities as a criterion for designating an Antarctic specially protected area. *Antarctic Science* 17, no. 1: 17–27. doi:10.1017/S0954102005002385.
- Soenen, S.A., D.R. Peddle, and C.A. Coburn. 2005. SCS+C: A modified sun-canopy-sensor topographic correction in forested terrain. *IEEE Transactions on Geoscience and Remote Sensing* 43, no. 9: 2148–59. doi:10.1109/TGRS.2005.852480.
- Sroková, S., and D. Nývlt. 2021. Bedload geochemical and petrophysical signature of the Algal and Bohemian streams, James Ross Island, Antarctic Peninsula. *Czech Polar Reports* 11, no. 2: 203–14. doi:10.5817/CPR2021-2-14.
- Staines, K.E.H., J.L. Carrivick, F.S. Tweed, A.J. Evans, A. J. Russell, T. Jóhannesson, and M. Roberts. 2015. A multi-dimensional analysis of pro-glacial landscape change at Sólheimajökull, southern Iceland. *Earth Surface Processes and Landforms* 40, no. 6: 809–22. doi:10.1002/esp.3662.
- Stringer, C. 2022. *Contemporary (2016–2020) land cover classification across West Antarctica and the McMurdo Dry Valleys (version 1.0)*. NERC EDS UK Polar Data Centre. doi:10.5285/5a5ee38c-e296-48a2-85d2-e29db66e5e24 [Data set].
- Stringer, C. 2025. *21st century land cover change across the major proglacial regions of West Antarctica and the McMurdo Dry Valleys (version 1.0)*. NERC EDS UK Polar Data Centre. doi:10.5285/d6721952-a9ab-4021-adc6-1ccb4d52f1f9 [Data set].
- Strother, S.L., U. Salzmann, S.J. Roberts, D.A. Hodgson, J. Woodward, W. Van Nieuwenhuyze, E. Verleyen, et al. 2015. Changes in Holocene climate and the intensity of Southern Hemisphere Westerly Winds based on a high-resolution palynological record from sub-Antarctic South Georgia. *The Holocene* 25, no. 2: 263–79. doi:10.1177/0959683614557576.
- Syvitski, J.P.M. 2002. Sediment discharge variability in Arctic rivers: Implications for a warmer future. *Polar Research* 21, no. 2: 323–30. doi:10.3402/polar.v21i2.6494.
- Tejedo, P., J. Benayas, D. Cajiao, B. Albertos, F. Lara, L. R. Pertierra, M. Andrés-Abellán, et al. 2016. Assessing environmental conditions of Antarctic footpaths to support management decisions. *Journal of Environmental Management* 177: 320–30. doi:10.1016/j.jenvman.2016.04.032.
- Tejedo, P., J. Benayas, D. Cajiao, Y.-F. Leung, D. De Filippo, and D. Liggett. 2022. What are the real environmental impacts of Antarctic tourism? Unveiling their importance through a comprehensive meta-analysis. *Journal of Environmental Management* 308: 114634. doi:10.1016/j.jenvman.2022.114634.
- Tewkesbury, A.P., A.J. Comber, N.J. Tate, A. Lamb, and P. F. Fisher. 2015. A critical synthesis of remotely sensed optical image change detection techniques. *Remote Sensing of Environment* 160: 1–14. doi:10.1016/j.rse.2015.01.006.
- Tichit, P., P. Brickle, R.J. Newton, P. Convey, and W. Dawson. 2024. Introduced species infiltrate early stages of succession after glacial retreat on sub-Antarctic South Georgia. *NeoBiota* 92: 85–110. doi:10.3897/neobiota.92.117226.
- Torres-Mellado, G.A., R. Jaña, and M.A. Casanova-Katny. 2011. Antarctic hairgrass expansion in the South Shetland archipelago and Antarctic Peninsula revisited. *Polar Biology* 34, no. 11: 1679–88. doi:10.1007/s00300-011-1099-6.
- Váczi, P., and M. Barták. 2022. Multispectral aerial monitoring of a patchy vegetation oasis composed of different vegetation classes. UAV-based study exploiting spectral reflectance indices. *Czech Polar Reports* 12, no. 1: 131–42. doi:10.5817/CPR2022-1-10.
- Váczi, P., M. Barták, M. Bednaříková, F. Hrbáček, and J. Hájek. 2020. Spectral properties of Antarctic and Alpine vegetation monitored by multispectral camera: Case studies from James Ross Island and Jeseníky Mts. *Czech Polar Reports* 10, no. 2: 297–312. doi:10.5817/CPR2020-2-22.
- Vaughan, D.G., G.J. Marshall, W.M. Connolley, C. Parkinson, R. Mulvaney, D.A. Hodgson, J.C. King, C.J. Pudsey, and J. Turner. 2003. Recent rapid regional climate warming on the Antarctic Peninsula. *Climatic Change* 60, no. 3: 243–74. doi:10.1023/A:1026021217991.
- Walker, D.A., F.J.A. Daniëls, N.V. Matveyeva, J. Šibík, M. D. Walker, A.L. Breen, L.A. Druckenmiller, et al. 2018. Circumpolar Arctic vegetation classification. *Phytocoenologia* 48, no. 2: 181–201. doi:10.1127/phyto/2017/0192.
- Walshaw, C.V., A. Gray, P.T. Fretwell, P. Convey, M. P. Davey, J.S. Johnson, and C. Colesie. 2024. A

- satellite-derived baseline of photosynthetic life across Antarctica. *Nature Geoscience* 17, no. 8: 755–62. doi:[10.1038/s41561-024-01492-4](https://doi.org/10.1038/s41561-024-01492-4).
- Wang, J.A., D. Sulla-Menashe, C.E. Woodcock, O. Sonnentag, R.F. Keeling, and M.A. Friedl. 2020. Extensive land cover change across Arctic-Boreal Northwestern North America from disturbance and climate forcing. *Global Change Biology* 26, no. 2: 807–22. doi:[10.1111/gcb.14804](https://doi.org/10.1111/gcb.14804).
- Wilkes, M.A., J.L. Carrivick, E. Castella, C. Ilg, S. Cauvy-Fraunié, S.C. Fell, L. Füreder, et al. 2023. Glacier retreat reorganizes river habitats leaving refugia for Alpine invertebrate biodiversity poorly protected. *Nature Ecology and Evolution* 7, no. 6: 841–51. doi:[10.1038/s41559-023-02061-5](https://doi.org/10.1038/s41559-023-02061-5).
- Xu, R., H. Lin, Y. Lü, Y. Luo, Y. Ren, and A. Comber. 2018. A modified change vector approach for quantifying land cover change. *Remote Sensing* 10, no. 10: 1578. doi:[10.3390/rs10101578](https://doi.org/10.3390/rs10101578).